Heliyon 10 (2024) e29093

Contents lists available at ScienceDirect

Heliyon

journal homepage: www.cell.com/heliyon

Research article

Shenshuai Yingyang Jiaonang ameliorates chronic kidney disease-associated muscle atrophy in rats by inhibiting ferroptosis mediated by the HIF-1α/SLC7A11 pathway

Liliang Ju [a,1], Jianxin Diao [a,1], Jiaxing Zhang [a,1], Fahong Dai [b], Hong Zhou [c,d], Zhongxiao Han [a], Rong Hu [a], Tingting Pei [a], Fujing Wang [a], Zhuoen He [a], Xiuqiong Fu [e], Mingqing Wang [a,**], Wei Xiao [a,f,***], Yun Ma [g,*]

[a] School of Traditional Chinese Medicine, Southern Medical University, Guangzhou, China
[b] Shenzhen Bao'an Chinese Medicine Hospital, Guangzhou University of Chinese Medicine, Shenzhen, China
[c] National Clinical Research Center for Kidney Disease, Nanfang Hospital, Guangzhou, China
[d] Guangdong Provincial Clinical Research Center for Kidney Disease, Guangzhou, China
[e] School of Chinese Medicine, Hong Kong Baptist University, Hong Kong, China
[f] Key Laboratory of Glucolipid Metabolic Disorder, Ministry of Education, Guangdong Pharmaceutical University, Guangzhou, China
[g] Clinical Pharmacy Center, Nanfang Hospital, Southern Medical University, Guangzhou, China

ARTICLE INFO

Keywords:
Traditional Chinese medicine
Chronic kidney disease
Ferroptosis
Network pharmacology
HIF-1α
Gpx4

ABSTRACT

Objective: Shenshuai Yingyang Jiaonang (SSYYJN), a traditional Chinese medicine formula, can ameliorate muscle atrophy associated with chronic kidney disease (CKD). However, its mechanisms of action remain unclear. This study is to investigate the molecular mechanisms involved in the effects of SSYYJN in ameliorating muscle atrophy associated with CKD in rats. Methods: The chemical compounds of SSYYJN were identified by UPLC-Q-Orbitrap HRMS. Considering the dose-response relationship of the identified compounds, male SD rats were randomly divided into Sham, Model, SSYYJN, and α-Keto Acid (KA) groups. Subsequently, we assessed the therapeutic and anti-ferroptotic effects of SSYYJN. Network pharmacology studies were used to predict the molecular mechanism of SSYYJN on ferroptosis and were further verified for accuracy.

Results: A total of 42 active compounds were identified from SSYYJN. SSYYJN alleviated muscle atrophy caused by CKD, as evidenced by changes in body weight, serum biochemical indices, mass and histopathology of the skeletal muscle, and the levels of MuRF1. SSYYJN reduced the levels of iron, MDA, and ROS, increased the levels of GSH, NAPDH, and Gpx4. Network pharmacology analysis indicated that SSYYJN exerted anti-ferroptotic effects that were closely related to the HIF-1α signaling pathway. Molecular protein and genetic test results showed that SSYYJN increased HIF-1α protein and increased SLC7A11.

Conclusions: SSYYJN attenuates muscle atrophy in CKD by inhibiting ferroptosis through the activation of the HIF-1α/SLC7A11 pathway and might be a promising traditional Chinese medicine for muscle atrophy in CKD.

* Corresponding author.
** Corresponding author.
*** Corresponding author. School of Traditional Chinese Medicine, Southern Medical University, Guangzhou, China.
E-mail addresses: mingqing@smu.edu.cn (M. Wang), xw7688@smu.edu.cn (W. Xiao), myxw1977@fimmu.com (Y. Ma).
[1] These authors contributed equally to this work.

https://doi.org/10.1016/j.heliyon.2024.e29093
Received 27 December 2023; Received in revised form 26 March 2024; Accepted 31 March 2024
Available online 15 April 2024

1. Introduction

Chronic kidney disease (CKD) has become a major public health problem across the world and affects approximately 10 % of the global population [1]. Progressive muscle atrophy is one of the serious complications of CKD, which is characterized by a reduced cross-sectional area of muscle fibers, increased protein decomposition and a reduction in muscle mass [2,3]. Muscle atrophy is strongly associated with a lower quality of life, disability and a greater risk of death in CKD patients [4]. The recurrence rate of this condition is estimated to range from 12 % to 29 %, placing a huge financial burden on patients [5,6]. Thus, the demand for developing specific medicines for muscle atrophy is increasing and has become an urgent clinical problem. Related studies have demonstrated that the mechanisms underlying muscle atrophy are associated with caspase-3, myostatin, oxidative stress, autophagy and the ubiquitin-proteasome system (UPS) [7,8]. An increasing number of studies have found that ferroptosis is involved in the pathogenesis of various diseases, including cancer, neurodegenerative diseases,and acute kidney injury [9,10]. Morever, ferroptosis was identified in age-related skeletal muscle atrophy [11]. However, the precise roles of ferroptosis in CKD-induced muscle atrophy are currently unknown. This paper will study the perspective of ferroptosis in CKD-induced muscle atrophy.

Ferroptosis is an iron-dependent and programmed form of cell death that was only discovered recently, which differs from the traditional form of cell death. In terms of cellular morphology, the ferroptosis results in a reduced mitochondrial volume, an increased density of the bilayer membrane, the reduction or disappearance of the mitochondrial crest, rupture and shrinkage of the mitochondrial outer membrane [12]. Mechanistically, ferroptosis is mainly caused by abnormal iron metabolism, excessive reactive oxygen species (ROS), an increase of lipid peroxides, and the downregulation of glutathione (GSH) and solute carrier family 7 member 11 (SLC7A11) [13]. The Fenton reaction is a key step in the process of ferroptosis, which causes the accumulation of lipid peroxides and leads to oxidative damage in the cells [14]. The initial product of this process is lipid hydroperoxide although this is followed by the subsequent production of malondialdehyde (MDA). As an intracellular reducing agent, nicotinamide adenine dinucleotide phosphate (NAPDH) can promote the elimination of lipid hydroperoxides, thus ensuring that reduced GSH remains available for glutathione peroxidase 4 (Gpx4) [15].This paper will detect markers related to ferroptosis of iron, MDA, ROS, GSH, NAPDH and Gpx4, confirm whether CKD-induced muscle atrophy has occurred ferroptosis.

According to the literature, traditional Chinese medicine (TCM) has a good therapeutic effect on skeletal muscle atrophy [16,17]. However, there are no relevant studies to prove that Chinese medicinal herbs with anti-muscle atrophy effects can affect ferroptosis in CKD-induced muscle atrophy. Renshen Yangrong decoction, which is recorded in the traditional Chinese medical book “Formulary of Peaceful Benevolent Dispensary”, is a widely used form of TCM. Shenshuai Yingyang Jiaonang (SSYYJN) is derived from Renshen Yangrong decoction and composed of *Astragalus membranaceus* (Fisch.) Bunge (Huangqi), *Atractylodes macrocephala* Koidz. (Baizhu), *Rheum palmatum* L. (Dahuang), *Glycyrrhiza uralensis* Fisch. (Gancao), *Codonopsis pilosula* (Franch.) Nannf. (Dangshen), *Poria cocos* (Schw.) Wolf (Fuling), *Eucommia ulmoides* Oliv. (Duzhong), *Angelica sinensis* (Oliv.) Diels (Danggui), *Amomum villosum* Lour. (Sharen). Approved by Guangdong Food and Drug Administration (batch number, Z20110193), SSYYJN has become the hospital preparation for the treatment of skeletal muscle atrophy of CKD in Zhujiang Hospital (Guangzhou, China), and won a national invention patent (patent number, CN1391947A). Our previous studies have confirmed that SSYYJN high (16 g/kg), medium (8 g/kg), and low (4 g/kg) doses can reduce the renal function indicators of CKD rats Serum creatinine (Scr), Urea nitrogen (BUN), blood β2-microglobulin, urine microalbumin, improve CKD rat skeletal muscle cell atrophy, among which the medium dose group has the best effect [18]. In this paper, a dose of 8 g/kg will be selected for pharmacodynamic experiments. Although SSYYJN has a good efficacy on CKD-induced muscle atrophy, however, the molecular mechanism of its therapeutic effect on CKD-induced muscle atrophy has not been fully elucidated.

Due to the large and complex composition of SSYYJN, it is difficult by traditional methods to determine the main active ingredients of SSYYJN. However, recent developments in ultra-high performance liquid chromatography-quadrupole-orbitrap high resolution mass spectrometry (UPLC-Q-Orbitrap HRMS) have provided a powerful technological method for analysing abundant components of SSYYJN. In this regard, Network pharmacology is highly advantageous as it can identify the multi-components and multi-targets of TCM.

In the present study, we used UPLC-Q-Orbitrap HRMS to identify the components of SSYYJN. Then, we established a CKD-induced model of muscle atrophy in rats and investigated the therapeutic and anti-ferroptotic effects of SSYYJN. In addition, we predicted the molecular mechanisms underlying the action of SSYYJN against ferroptosis based on network pharmacology analysis and verified these predictions experimentally.

Table 1
The relevant information of nine constituent herbs in SSYYJN.

Chinese name	Botanical name	Weight (g)	Part used	Batch number	Herbal-producing region
Huangqi	*Astragalus membranaceus* (Fisch.)	25	Root	201001–2	Gansu
Baizhu	*Atractylodes macrocephala* Koidz	10	Rhizome	210502–1	Anhui
Dahuang	*Rheum palmatum* L.	10	Root	200601–7	Sichuan
Gancao	*Glycyrrhiza uralensis* Fisch.	5	Root and rhizome	20210301	Neimenggu
Dangshen	*Codonopsis pilosula* (Franch.) Nannf	25	Root	20210401	Gansu
Fuling	*Poria cocos* (Schw.) Wolf	15	Sclerotia	201201–3	Yunnan
Duzhong	*Eucommiae ulmoides* Oliv.	15	Root bark	20201201	Sichuan
Danggui	*Angelicae Sinensis* (Oliv.) Diels	10	Root	201101–3	Gansu
Sharen	*Amomum villosum* lour.	10	Ripe seed	201203–4	Guangdong

Table 2
Forward and reverse primers sequence.

Primer name	Sequence (5'→3')	
HIF-1α	Forward	ACTGATTGCATCTCCACCTTCT
	Reverse	TCGCTTCCTCTGAGCATTCT
Gpx4	Forward	TGGGAAATGCCATCAAATG
	Reverse	CGGCAGGTCCTTCTCTATCA
SLC7A11	Forward	TGCTGGCTTTTGTTCGAGTCT
	Reverse	GCAGTAGCTCCAGGGCGTA
GAPDH	Forward	GACAACTTTGGCATCGTGGA
	Reverse	ATGCAGGGATGATGTTCTGG

2. Material and methods

2.1. Identifying the composition of SSYYJN by UPLC-Q-orbitrap HRMS

Information relating to the nine constituent herbs in SSYYJN is shown in Table 1. The plant name has been checked with http://www.theplantlist.org. All herbs were acquired from the pharmacy of TCM, Nanfang Hospital, Southern Medical University (Guangzhou, China), and were authenticated by Professor Chuanming Liu from the School of TCM at Southern Medical University. Then, the nine herbs were extracted using deionized water and lyophilized using a freeze dryer. In brief, all herbs were mixed and immersed in a 10-fold volume of deionized water for 30 min and were then deconcocted in boiling water for 1 h. This process was repeated twice. The two extracts were then mixed and evaporated under reduced pressure. The concentrated solution was then freeze-dried to powder at −20 °C. Then, we accurately weighed 0.05 g of powder and dissolved the powder in a mixed solution of methanol and water (volume ratio: 2:3) for extraction. Then, the mixture was centrifuged at 15,000 g for 20 min and 1 μL of the supernatant was injected for UPLC-Q-Orbitrap HRMS analysis.

The chromatographic separation of the sample was carried out on an UltiMate 3000 UPLC system (Thermo Fisher Scientific, Germany). We used a Waters C18 column (2.1 mm × 100 mm, 1.8 μm) at 45 °C using (A) 0.1 % formic acid water and (B) acetonitrile (containing 0.1 % formic acid) as the mobile phase for gradient elution. Gradient elution was performed at a flow rate of 0.3 mL/min as follows: 0–18 (2%–50 % B), 18–21 (50%–95 % B), 21–23 (95 % B), 23–23.1 (95%–5% B) and 23.1–25 (2 % B); the injection volume was 1 μL. Mass spectrometric detection was performed using a hybrid quadrupole orbitrap high-resolution mass spectrometer (Q Exactive, Thermo Fisher Scientific, MA, United States) equipped with a heated electrospray ion source (HESI). The various instrumental settings were as follows for both positive and negative ion-mode electrospray ionization: the mass range was m/z 70∼1050 Da with a full scan MS resolution of 70,000; the capillary voltage for positive and negative ionization were 3500 and 3000 V; sheath gas was set to 35 psi, auxillary gas was set to 10 psi, and the spray temperature was 350 °C. The original data were analyzed by Xcalibur 3.0 software (Thermo Fisher Scientific, FL, United States) and Compound Discoverer 3.1 software coupled to mzCloud and ChemSpider databases.

2.2. Animal modeling and grouping

All animal manipulations were approved by the Ethics Committee of Southern Medical University (No. SMUL2021012). Male Sprague-Dawley (SD) rats (250–350 g) were supplied by the Laboratory Animal Centre of Southern Medical University (Guangzhou, China). The rats were housed under a constant 12-h light-dark cycle at 25 ± 2 °C and had free access to water and food. To establish the model of CKD, we performed 5/6 nephrectomy by a two-step procedure as described previously [19]. The entire operation was performed aseptically; After 5/6 nephrectomy for 7 weeks, we determined the serum levels of creatinine (Scr), blood urea nitrogen (BUN), albumin (ALB), Hemoglobin (Hb), and also recorded body weight, so that we could judge whether the CKD-induced muscle atrophy model had been established successfully. All SD rats were randomly assigned into four groups (n = 8): a sham group, a model group, a model + SSYYJN group and a model + compound α-Keto Acid Tablets (KA) group. Our previous studies have demonstrated that high (16 g/kg), medium (8 g/kg) and low (4 g/kg) doses of SSYYJN can improve renal function and malnutrition levels (Table SI, Table S2). In this paper, the therapeutic doses of the drugs were calculated based on human and rat equivalent dose ratios. The dosage of SSYYJN formula is 125 g. Calculated based on an adult's body weight of 60 kg, the daily dosage for adults is 125 g/60 kg/d. According to the guidelines for dose conversion between rats and humans, the conversion coefficient is 6.3. Therefore, the daily dosage for rats is 13.125 g/kg/d. The clinical adult dose of KA is 7.56–15.12 g/d, similarly, the daily dosage for rats is 0.7938–1.5876 g/kg/d, and the median dose is 1.2 g/kg/d. SSYYJN and KA were administered orally as a suspension for 7 weeks. Rats in the sham and model group were given the same amount of deionized water.

2.3. Biochemical parameters

All rats were sacrificed with pentobarbital sodium after completion of the treatment, blood was centrifuged at 1500 g for 15 min to obtain serum. Serum biochemical indicators (Scr, BUN, Cystatin C, and ALB) and Hb level in the blood were all detected by appropriate kits (Nanjing Jiancheng Bioengineering Institute, China) according to the manufacturer's protocol.

2.4. Hematoxylin and Eosin staining (H&E)

Histopathological examination was performed to observe the microstructure of the kidney and TA muscle in experimental rats. Standard histopathological examination protocols were used. In brief, tissues were first fixed and embedded, and then dewaxed, gradually hydrated, stained sequentially with Hematoxylin and Eosin, dehydrated with a graded series of alcohols and then sealed with neutral glue. The sections were photographed with a Leica microscope (Lax X, Leica, Germany) and quantified by Image J 1.53 software (National Institute of Mental Health, USA).

2.5. Masson's trichrome staining

Kidney tissue was fixed with 4 % paraformaldehyde, embedded and cut into sections that were 4 μm thick. The slides were then subjected to conventional dewaxing to water. Fibrotic pathological alterations in the rat kidney tissue were determined using a Masson's Stain Kit (Nanjing Jiancheng Bioengineering Institute, China) based on the manufacturer's protocol. Renal tissue and fibrotic

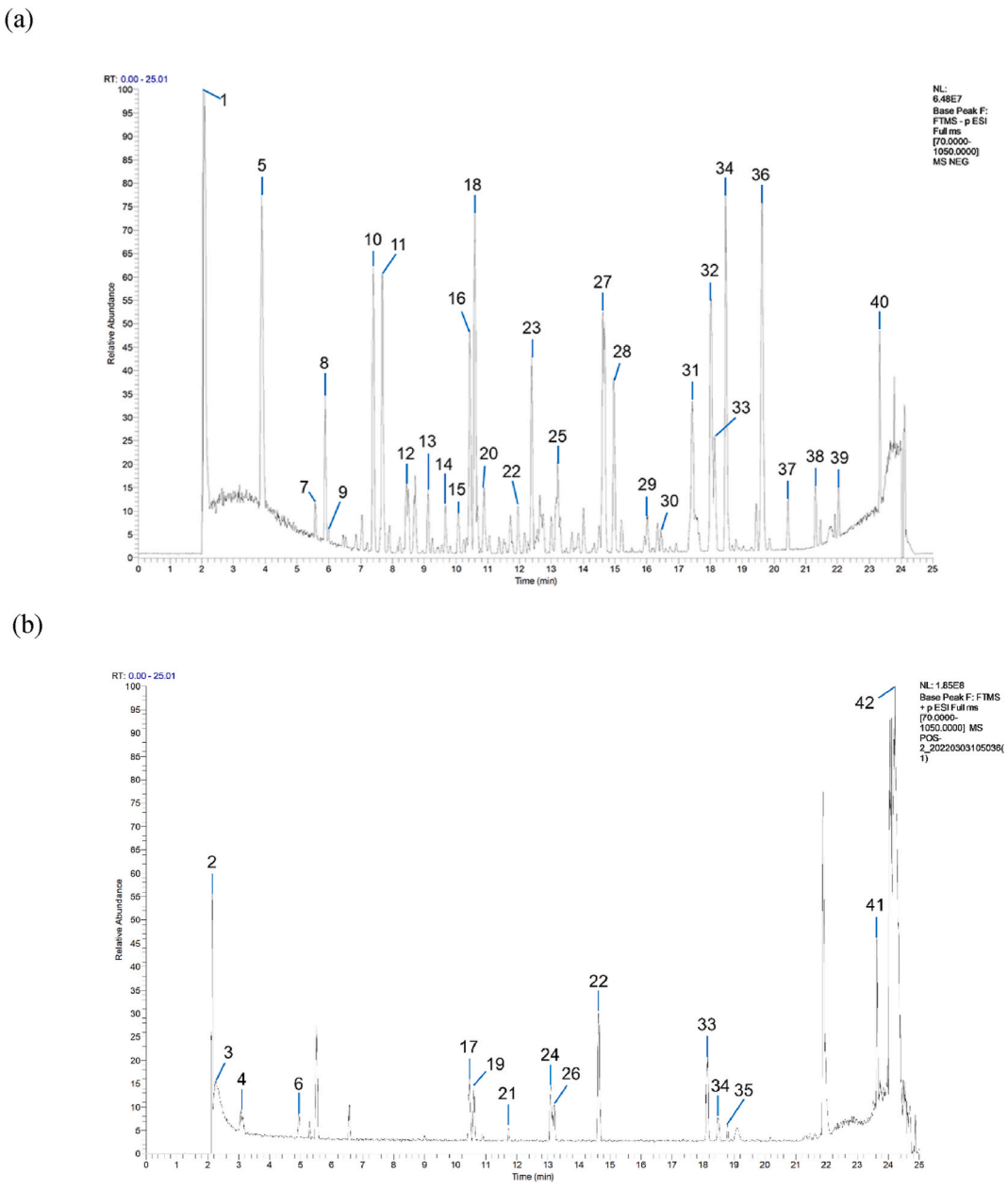

Fig. 1. Base peak ion flow diagram showing the components of SSYYJN in negative (a) and positive (b) ion mod.

Table 3
Identification of chemical compounds within SSYYJN by UPLC-Q-Orbitrap HRMS.

NO.	Rt (min)	Aduct	Extraction mass (Da)	Error (ppm)	Formula	Identification	MS^2 ions	Source	Class
1	2.09	–	192.02601	−5.15	$C_6H_8O_7$	Citric acid	(−) 191.01878[M − H]-,173.00793,154.99706, 129.01799, 111.00747, 87.00740, 85.02814, 57.03326	[48]	Organic acid
2	2.12	+	138.03120	−3.62	$C_7H_6O_3$	Protocatechuic aldehyde	(+) 139.98743[M+H]+, 116.97192, 113.96393, 111.09175, 98.09653, 85.50272, 70.06572, 57.93544	[49]	Phenylpropanoid
3	2.27	+	135.05489	2.96	$C_5H_5N_5$	Adenine	(+) 136.02104[M+H]+, 109.01087, 95.04939, 91.56100, 79.62068, 71.93567, 65.03894, 60.95022	[50]	Alkaloids
4	3.07	+	267.09554	−4.53	$C_{16}H_{29}NO_2$	Adenosine	(+) 268.10281[M+H]+, 136.06158, 131.38133, 119.03541, 94.04070, 85.02869, 69.03400, 57.03428	[51]	Alkaloids
5	3.89	–	170.02035	−6.88	$C_7H_6O_5$	Gallic acid	(−) 169.01306[M − H]-, 125.02321, 107.01272, 97.02807, 81.03321, 69.03325	[51]	Organic acid
6	4.93	+	165.07836	−3.95	$C_9H_{11}NO_2$	L-Phenylalanine	(+) 166.08563[M+H]+, 149.05949, 131.04900, 120.08079, 103.05446, 93.07012, 79.05473	[52]	Amino acids
7	5.57	–	316.07930	−0.42	$C_{13}H_{16}O_9$	Protocatechuate glucoside	(−) 315.07208[M − H]-, 152.01039, 133.02808, 108.02041, 85.02808, 71.01267	[53]	Organic acid
8	5.89	–	374.12105	−0.64	$C_{16}H_{22}O_{10}$	Geniposidic acid	(−) 373.11377[M − H]-, 335.07434, 314.25082, 211.06056, 193.04994, 167.07024, 149.05969, 123.04388, 105.03315, 89.02302, 71.01251	[54]	Organic acid
9	5.98	–	154.02545	−7.55	$C_7H_6O_4$	Protocatechuic acid	(−) 153.01814[M − H]-, 109.02823, 103.09509, 81.03329, 65.35208	[52]	Organic acid
10	7.44	–	166.06230	−4.21	$C_9H_{10}O_3$	3′,4′-Dihydroxyphenylacetone	(−) 165.05449[M − H]-, 142.80841, 121.06446, 119.04913, 105.10963, 93.03295, 81.99586, 70.90002, 59.01250	[49]	Phenylpropanoid
11	7.68	–	290.07865	−1.33	$C_{15}H_{14}O_6$	Catechin	(−) 289.07150[M − H]-, 245.08170, 221.08127, 203.07045, 151.03883, 137.02319, 123.04380, 109.02824, 97.02814, 83.01231	[55]	Tannins
12	8.54	–	168.04114	−6.6	$C_8H_8O_4$	Homogentisic acid	(−) 167.03386[M − H]-, 152.01059, 123.04389, 108.02077, 95.04896, 64.40240	[49]	Organic acid
13	9.11	–	682.24745	0.47	$C_{32}H_{42}O_{16}$	Pinoresinol diglucoside	(−) 681.24017[M − H]$^-$, 519.18671, 357.13446, 342,11154, 151.03900, 136.01541, 121.02818	[56]	Lignans
14	9.66	–	543.3353	5.88	$C_{33}H_{51}O_6$	25-Hydroxypachymic acid	(−) 542.15137[M − H]-, 526.96692, 400.57474, 264.91934, 213.84070, 167.93512, 61.98699	[57]	Organic acid
15	10.07	–	164.04714	−1.28	$C_9H_8O_3$	(E)-*p*-hydroxycinnamic acid	(−) 163.03899[M − H]$^-$, 125.37830, 119.04898, 113.91008, 93.03350, 68.05715, 56.26588	[58]	Organic acid
16	10.44	–	432.10565	−1.19	$C_{21}H_{20}O_{10}$	Aloe-emodin-8-*O*-β-D-glucoside	(−) 431.09790[M − H]-, 293.04565, 269.04547, 240.04260, 239.03452, 225.05548	[55]	Anthraquinone
17	10.46	+	446.11952	−2.58	$C_{22}H_{22}O_{10}$	Calycosin-7-*O*-β-D-glucoside	(+) 447.12680[M+H]$^+$, 285.07516, 270.05161, 253.04886, 225.05409, 214.06149, 137.02313	[59]	Flavonoids
18	10.59	–	418.12599	−1.25	$C_{21}H_{22}O_9$	Liquiritin	(−) 417.11871[M − H]-, 255.06604, 153.01822, 135.00757, 119.04897, 91.01756	[60]	Flavonoids
19	10.60	+	256.07234	−4.68	$C_{15}H_{12}O_4$	DL-liquiritigenin	(+) 257.07962[M+H]$^+$, 239.06941, 211.07500, 163.03850, 155.03386, 147.04381, 137.02313, 119.04912,	[53]	Flavonoids
20	10.88	–	356.12578	−0.62	$C_{20}H_{20}O_6$	Sigmoidin B	(−) 355.10324[M − H]$^-$, 261.33701, 245.98561, 189.05461, 161.05954, 147.04410, 113.02337, 85.02828, 71.01245, 59.01247	[61]	Flavonoids
21	11.72	+	234.12470	−3.84	$C_{14}H_{18}O_3$	Lobetyol	(+) 235.09546[M+H]$^+$, 217.08566, 193.07440, 191.06995, 176.04619, 151.03879, 135.08026, 67.01840	[52]	Others
22	11.94/ 14.63	−/+	284.06822	−0.88	$C_{16}H_{12}O_5$	Calycosin	(−) 283.06097[M − H]$^-$, 268.03775, 239.03474, 211.03954, 184.05223, 148.01555, 135.00760 (+) 285.07437[M+H]+, 270.05151, 253.04881, 225.05396, 213.05426, 197.05913, 186.06676, 137.02318, 134.03606	[59]	Flavonoids
23	12.38	–	188.10388	−5.16	$C_9H_{16}O_4$	Azelaic acid	(−) 187.09660[M − H]-, 159.87828, 141.86707, 125.09595, 97.06444, 57.03325	[52]	Organic acid

(*continued on next page*)

Table 3 (*continued*)

NO.	Rt (min)	Aduct	Extraction mass (Da)	Error (ppm)	Formula	Identification	MS^2 ions	Source	Class
24	13.08	+	182.05790	−0.05	$C_9H_{10}O_4$	3,5-dimethoxy-4-Hydroxybenzaldehyde	(+) 183.07722[M+H]+, 168.98112, 155.04637, 127.01534, 116.99469, 98.9843	[49]	Others
25	13.20	–	462.11610	−0.24	$C_{22}H_{22}O_{11}$	1-*O*-galloyl-2-*O*- cinnamoyl-β-D-glucoside	(−) 461.10883[M − H]$^-$, 401.08597, 313.05664, 254.05371, 211.02463, 169.01311, 147.04391, 123.00752, 85.02817	[55]	Tannins
26	13.21	+	430.12444	−3.07	$C_{22}H_{22}O_9$	Ononin	(+) 431.13171[M+H]$^+$, 269.08020, 254.05650, 237.05409, 213.09055, 197.05917, 118.04130	[59]	Flavonoids
27	14.65	–	432.10515	−1.22	$C_{21}H_{20}O_{10}$	Emodin-8-*O*-β-D-glucoside	(−) 431.09787[M − H]$^-$, 269.04550, 225.05522, 210.03192, 197.05948, 181.06424	[55]	Anthraquinone
28	14.97	–	416.11041	−0.79	$C_{21}H_{20}O_9$	Chrysophanol-8-*O*-β-D-glucoside	(−) 415.10312[M − H]$^-$, 277.05054, 266.05765, 239.07068, 225.05522	[51]	Anthraquinone
29	16.01	–	330.23886	−5.35	$C_{18}H_{34}O_5$	(15Z)-9,12,13-trihydroxy-15-octadecenoic acid	(−) 329.13922[M − H]$^-$, 243.06946, 219.10146, 207.10199, 185.63698, 137.02307, 122.03604, 109.02834, 93.03339	[49]	Organic acid
30	16.44	–	838.39882	0.13	$C_{42}H_{62}O_{17}$	Licoricesaponin G	(−) 837.39154[M − H]$^-$, 643.34650, 351.05664, 193.03462, 175.02345, 113.02314, 85.02819	[61]	Triterpenoids
31	17.43	–	330.24049	−0.42	$C_{18}H_{34}O_5$	9,12,13-trihydroxy-10-octadecenoic acid	(−) 329.23322[M − H]$^-$, 293.21182, 229.14406, 211.13344, 171.10167, 139.11176, 127.11167, 99.08018, 57.03329	[62]	Organic acid
32	18.02	–	298.04741	−1.11	$C_{16}H_{10}O_6$	Rhein methyl ester	(−) 297.04013[M − H]$^-$, 253.05051, 225.05518, 210.03149, 109.11985, 79.90932	[55]	Anthraquinone
33	18.14	+/−	268.07332	−3.67	$C_{16}H_{12}O_4$	Formononetin	(+) 269.07960[M+H]$^+$, 269.08014, 237.05400, 226.06168, 213.09045, 107.04939, 118.04136, 154.02525, 181.06419, 197.05925	[59]	Flavonoids
34	18.49	+/−	822.40394	−0.57	$C_{42}H_{62}O_{16}$	Glycyrrhizic acid	(−) 821.39667[M − H]$^-$, 351.05682, 193.03467, 175.02396, 113.02311 (+) 823.40759[M+H]+, 647.37952, 471.34653, 453.33539, 435.32562, 217.15831, 175.14764, 121.10112, 95.08580, 81.07030	[53]	Triterpenoids
35	18.80	+	273.26543	−4.94	$C_{16}H_{35}NO_2$	Lauryldiethanolamine	(+) 274.27271 [M+H]$^+$, 256.26257, 215.48579, 106.08649, 88.07605, 70.06562, 57.07043	[50]	Others
36	19.63	–	284.03172	1.29	$C_{15}H_8O_6$	Rheic acid	(−) 283.02444[M − H]$^-$, 257.04538, 239.03462, 211.03951, 183.04430, 167.04912	[51]	Anthraquinone
37	20.44	–	590.14241	−0.03	$C_{24}H_{26}N_6O_{10}S$	1-methyl-8-hydroxy-9,10-anthraquinone -3-*O*-(6′-*O*-cinnamoyl)-glucoside	(−) 589.13507[M − H]$^-$, 295.06201, 266.05841, 253.05054, 225.05533	[55]	Anthraquinone
38	21.31	–	312.08377	−2.4	$C_{14}H_{16}O_8$	Ellagic acid	(−) 311.22272[M − H]$^-$, 293.21252, 235.17072, 223.16992, 201.11244, 87.04375	[56]	Organic acid
39	22.04	–	314.24562	−0.29	$C_{18}H_{34}O_4$	9,10-dihydroxy-12-octadecenoic acid	(−) 313.23834[M − H]$^-$, 277.21747, 201.11255, 171.10181, 127.11165, 58.00471	[52]	Organic acid
40	23.34	–	298.25047	−1.08	$C_{16}H_{10}O_6$	6-methyl-rhein	(−) 297.24319[M − H]$^-$, 279.23267, 256.98337, 194.45506, 183.13821, 113.09624	[63]	Anthraquinone
41	23.63	+	148.05190	−3.58	$C_9H_8O_2$	Cinnamic acid	(+) 149.02257[M+H]$^+$, 121.02829, 111.04401, 93.03383, 67.02957, 65.03918	[64]	Organic acid
42	24.21	+	122.03650	−2.29	$C_7H_6O_2$	4-Hydroxybenzaldehyde	(+) 123.07868[M+H]$^+$, 100.39412, 88.95665, 82.05295, 70.41364, 60.04245, 51.81756	[49]	Others

Rt: Retention time.

tissue were stained red and blue, respectively, by Masson's trichrome staining.

2.6. Immunohistochemical analysis

Sections of TA muscle were dewaxed, rehydrated and then pre-treated by microwave antigen retrieval in sodium citrate buffer (Boster, Wuhan, China). Then, the sections were soaked in 3 % hydrogen peroxide for 15 min and then blocked in 5 % bovine serum albumin (BSA) for 20 min. The sections were then incubated overnight with a muscle ring-finger-1 (MuRF1) antibody (1:100, Affinity, USA) at 4 °C. On the second day, the subsequent operations were carried out according to the protocol of the immunochromogenic kit (Gene Tech, Shanghai, China). In brief, the slides were washed and add 100 μL of enzyme-labeled anti-rabbit IgG polymer for 30 min. 3,3N-diaminobenzidine tetrahydrochloride (DAB) was added to the sections which were then stained with hematoxylin. Finally, positive staining was detected by microscopy (Lax X, Leica, Germany).

2.7. Iron parameters

Tissue non-heme iron was detected by a Tissue Iron Assay Kit produced by Nanjing Jiancheng Bioengineering Institute (Nanjing, China) in accordance with the manufacturer's protocol. In brief, we weighed tissue into a grinding tube and added a certain volume of normal saline according to a weight (g): volume (ml) ratio of 1:9. Then, the tissue was minced and mechanically homogenized in an ice bath and centrifuged at 1000 g for 10 min. Finally, the supernatant was aspirated for analysis.

2.8. NADPH assay

NADPH levels were detected with a Coenzyme II (NADP/NADPH) Content Test Kit (Nanjing Jiancheng Bioengineering Institute, Nanjing, China). Tissues were homogenized in an alkaline extraction solution on ice and incubated at 95 °C for 5 min. The homogenate was then cooled in an ice bath and centrifuged at 10,000 g for 10 min at 4 °C. The supernatant was then mixed with NADP extraction solution and centrifuged at 10,000 g for 10 min at 4 °C to collect the supernatant. Then, we added NADPH reaction solution and mixed thoroughly; this was allowed to stand at room temperature for 20 min in the dark. Absorption was then detected at 570 nm on a microplate reader (Gen5, BioTek, Winooski, VT, USA).

2.9. Assessment of MDA and GSH levels

The levels of GSH in TA muscles were tested with a Reduced Glutathione (GSH) Assay Kit (Nanjing Jiancheng Bioengineering Institute, Nanjing, China). The levels of MDA were detected with a Malondialdehyde (MDA) Assay Kit (Nanjing Jiancheng Bioengineering Institute, Nanjing, China) in accordance with the manufacturer's protocols.

2.10. ROS production assay

The levels of ROS were detected with a ROS Assay Kit (Beyotime, Shanghai, China) in accordance with the manufacturer's protocol. Tissue sections were subjected to conventional dewaxing to water. The sections were then treated with dihydroethidium at 37 °C for 30 min in the dark. These sections were then washed with PBS buffer and counterstained with DAPI; nuclei were stained blue and ROS were stained red. Then, we capetured images by fluorescence microscopy (Lax X, Leica, Germany).

2.11. Network pharmacology analysis

The chemical components of SSYYJN were downloaded from the traditional Chinese medicine systems pharmacology database (TCMSP, http://lsp.nwu.edu.cn/tcmsp.php).We used an oral bioavailability (OB) $\geq$ 30 % and drug-likeness (DL) $\geq$ 0.18 as criteria to identify the active ingredients of SSYYJN; 140 active compounds were identified.

Next, we obtained the SMILE structural formula of the screened active compounds from the PubChem database (https://pubchem.ncbi,nlm.nih.gov/); these were then submitted to Swiss target prediction (http://www.swisstargetprediction.ch/) with the species set to homo sapiens. Potential targets were predicted for each component of SSYYJN. Targets related to CKD-PEW were acquired from GeneCards (https://www.genecards.org/) and DisGENET (https://www.disgenet.org/) databases(The data obtained by GeneCards has been exempted by the Medical Ethics Committee of the Hospital of Integrated Traditional Chinese and Western Medicine of Southern Medical University). Genes associated with ferroptosis were acquired from the FerrDB (http://www.zhounan.org/ferrdb/) database. An herb-compound-target network of SSYYJN was established by inputting the potential targets of the 140 identified components into Cytoscape 3.8.0 software (http://www.cytoscape.org/).

By identifying the intersection for the potential targets of SSYYJN, CKD-PEW-related genes, and ferroptosis-related genes, we obtained the targets of SSYYJN that were involved in the inhibition of ferroptosis in CKD-PEW. The common genes were then imported into the STRING (Version 11.5) database for protein-protein interaction (PPI) analysis. The results were visualized by Cytoscape 3.8.0. Degree values for common genes were calculated by the CytoNCA plug-in and the hub genes for the inhibitory action of SSYYJN on ferroptosis in CKD-PEW were obtained according to degree values.

The Bioconductor package in R language software was used for Gene Ontology (GO) and Kyoto Encyclopedia of Genes and Genomes (KEGG) enrichment analysis. GO analysis mainly involved three aspects: molecular function (MF), biological process (BP) and

cellular components (CC). A q value < 0.05 was set as a threshold and the top 27 categories were selected and plotted as bubble charts with R Studio software.

2.12. Real-time quantitative PCR (RT-qPCR)

Total RNA was extracted from TA muscles with TRIZOL reagent (Solarbio, Beijing, China). Then, 500 ng of total RNA was converted into cDNA using PrimeScript RT reagent (Takara, Shiga, Japan). PCR was then performed using a SYBR Green PCR kit (Accurate biology, Hunan, China) and the reactions were run in a LightCycler 96 instrument (Basle, Switzerland). Using GAPDH as a control, the expression levels of target genes were calculated with the $2-\Delta\Delta Ct$ method. The primer sequences are listed in Table 2.

2.13. Western Blot (WB) analysis

TA muscle tissue samples were lysed in an ice-cold mixture of RIPA lysis buffer and protease inhibitor cocktail (Solarbio, Beijing, China) for 30 min. The lysate was then centrifuged (12,000 g, 10 min, 4 °C) and the supernatant was collected. The protein concentration of each supernatant was determined by the BCA protein assay (Beyotime, Shanghai, China). Each protein sample (28 μg) was then separated by 12.5 % SDS-PAGE and transferred to polyvinylidene difluoride (PVDF) membranes (Millipore, Burlington, MA, USA). Next, 5 % non-fat milk dissolved in Tris-buffered saline containing Tween-20 (TBST) was used to block non-specific binding for 1.5 h. Next, the membranes were incubated overnight at 4 °C with a range of primary antibodies: anti-SLC7A11 (1:1000, Abcam, Cambridge, UK), anti-Gpx4 (1:1000, Abcam, Cambridge, UK), anti–HIF–1 α (1:2000, Bioss, Beijing, China) and anti-GAPDH (1:10000, Cell Signaling Technology, Danvers, MA, USA). The following day, appropriate anti-rabbit secondary antibodies (1:1000, Proteintech, Chicago, USA) were incubated with the sections at room temperature for 1.5 h. Positive signals were then detected with an enhanced chemiluminescence detection system (Millipore, Burlington, MA, USA) and the target bands were analyzed by Image J 1.53 software (National Institute of Mental Health, USA).

2.14. Immunofluorescence staining

After routine dewaxing and rehydration, tissue sections were immersed in sodium citrate buffer (Boster, Wuhan, China) for antigen repair at 100 °C for 10 min. The tissue sections were then washed with PBS and permeabilized in 2 % Trixon-100 solution for 10 min. Non-specific binding was blocked with 5 % goat serum. A primary antibody against HIF-1α (1:200; Bioss, Beijing, China) was then incubated with TA muscle sections overnight at 4 °C. The following morning, a 488-conjugated secondary antibody (1:200; Baiqiandu, Wuhan, China) was incubated with the sections in the dark for 2 h. The sections were then re-washed and incubated with DAPI (Beyotime, Shanghai, China) in the dark. Finally, images were acquired with an inverted fluorescence microscope (Lax X, Leica, Germany) and semi-quantitative analysis was performed with Image J 1.53 software (National Institute of Mental Health, USA).

2.15. Statistical analyses

Experimental data are presented as a mean ± standard deviation (SD). Statistical analysis was carried out with SPSS 26.0 software (Media Cybernetics, Inc., Rockville, MD, USA). Values between two groups were compared with the Student's t-test. Multiple comparison tests were performed by one-way analysis of variance (ANOVA) and the Least Significance Difference (LSD) post hoc test. Figures were created by GraphPad Prism 8.0 software (GraphPad Software Inc., San Diego, CA, USA) and $P < 0.05$ was considered statistically significant.

3. Results

3.1. Identification of the chemical components of SSYYJN by UPLC-Q-orbitrap HRMS

The active components of SSYYJN were separated and verified by UPLC-Q-Orbitrap HRMS and a total ion current (TIC) diagram was acquired in both positive (Fig. 1a) and negative (Fig. 1b) ion modes. Based on the Compounds Discover database and the available literature, we identified 42 chemical components (Table 3), including 14 organic acids and their glycosides, 7 Anthraquinone, 7 Flavonoids, 2 Tannins, 2 Alkaloids, 2 Triterpenoids, 2 Phenylpropan-oid, 1 Amino acids, 1 Lignans and 4 others.

3.2. Ferroptosis was found in CKD-associated muscle atrophy and SSYYJN could inhibit ferroptosis

The experimental procedure is presented in Fig. 2A. First, SSYYJN treatment improved renal function in rats with CKD-induced muscle atrophy, this was consistent with previously reported results.[27,28] Compared with the sham group, the levels of Scr and Cystatin C were markedly increased ($P < 0.01$) in rats with CKD-induced muscle atrophy, but decreased ($P < 0.01$) significantly after the administration of SSYYJN and KA (Fig. 2B and C). HE and Masson's trichrome staining was used to analyze the pathology of the renal tissue. The renal tissue of rats in the sham group was normal; however, there were serious lesions in the kidneys of rats in the model group, including renal tubular dilatation, renal fibrosis, and inflammatory cell infiltration. Renal pathology was significantly improved in the SSYYJN and KA group (Fig. 2D). The levels of Hb and ALB were reduced ($P < 0.01$) in the model group when compared with the sham group but were increased ($P < 0.01$) after SSYYJN and KA treatment (Fig. 2E and F).

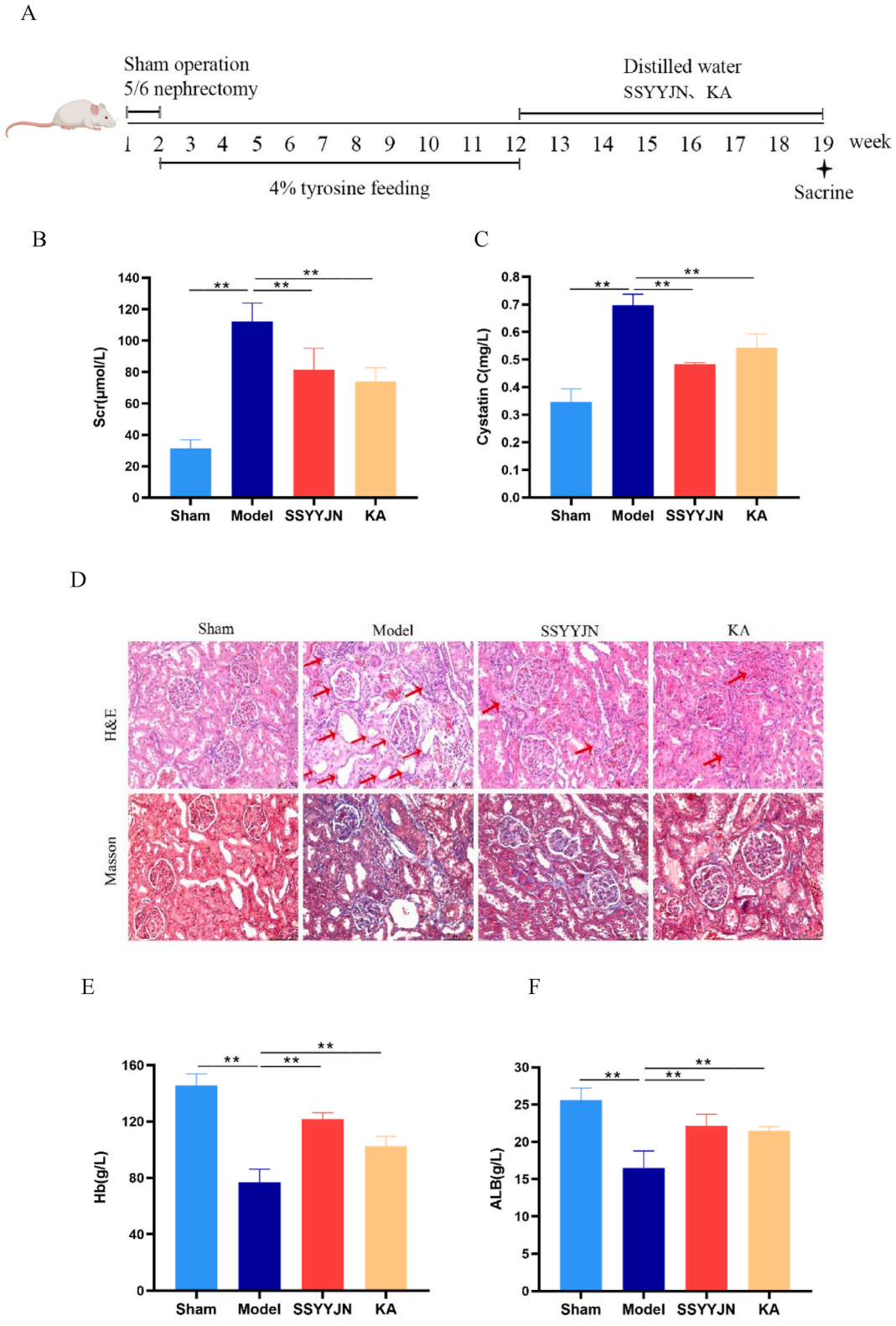

Fig. 2. Effect of SSYYJN on renal function in rats with CKD-induced muscle atrophy. Schematic protocol for the animal experiment (A). The levels of Scr (B), Cystatin C (C), Hb (E) and ALB (F) in the serum of rats in different groups. Representative images of H&E and Masson trichrome (D) statining from kidney sections (200X). Data are presented as mean ± SD for 6 rats in each group. *P < 0.05, **P < 0.01.

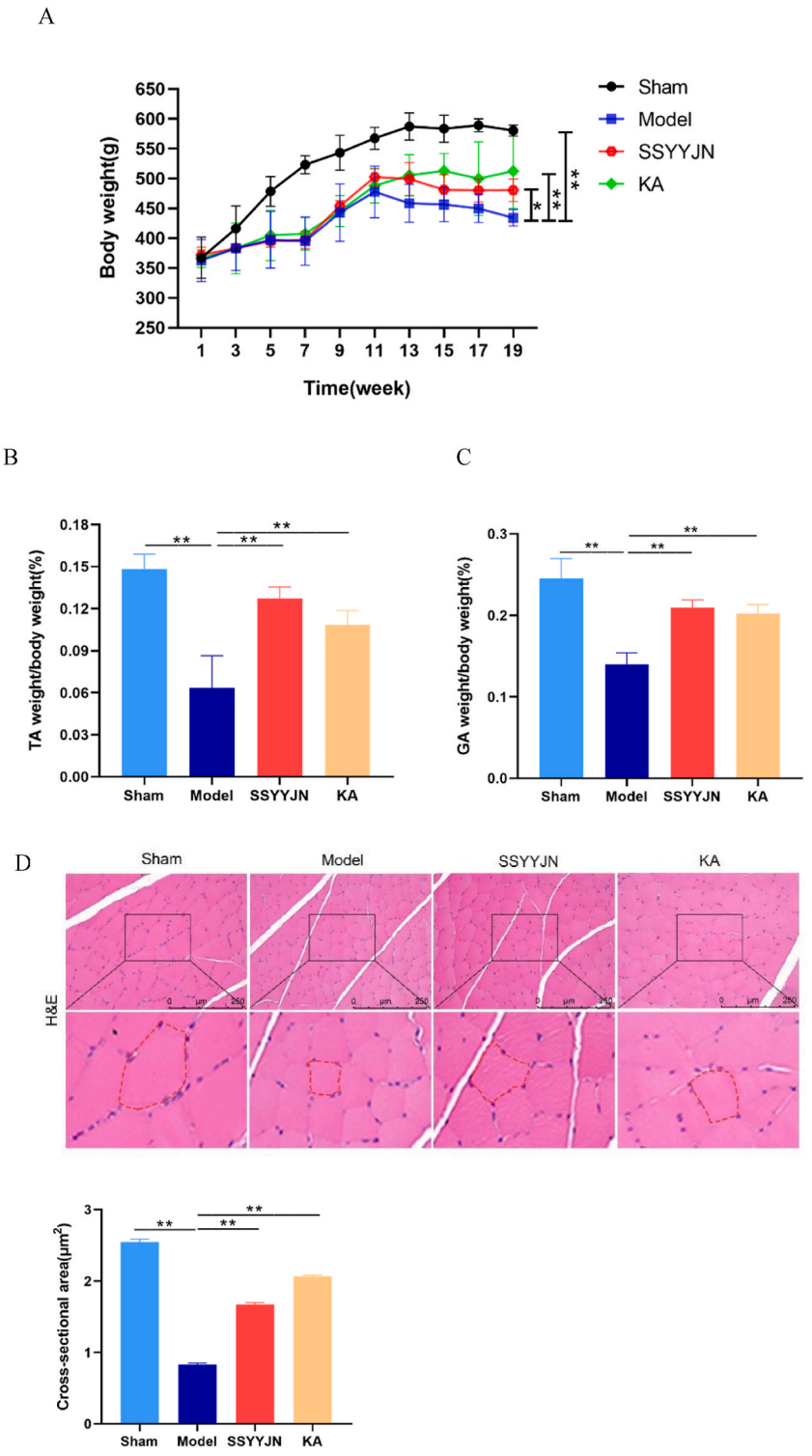

Fig. 3. Effect of SSYYJN on muscle atrophy in CKD-induced muscle atrophy rats. (A) Body weight was measured every two weeks during the 19-week experiment. (B–C) The weight of GA and TA muscle were normalized to body weight. (D) Sections of TA muscle were observed by H&E staining and images were taken at a magnification of 200 × . The mean fiber size was determined by Image J. (E–F) Representative images of IHC and WB of MuRF1 in rat TA muscle and statistical analysis of WB data. Data are presented as mean ± SD for 3–8 rats in each group. *P < 0.05, **P < 0.01.

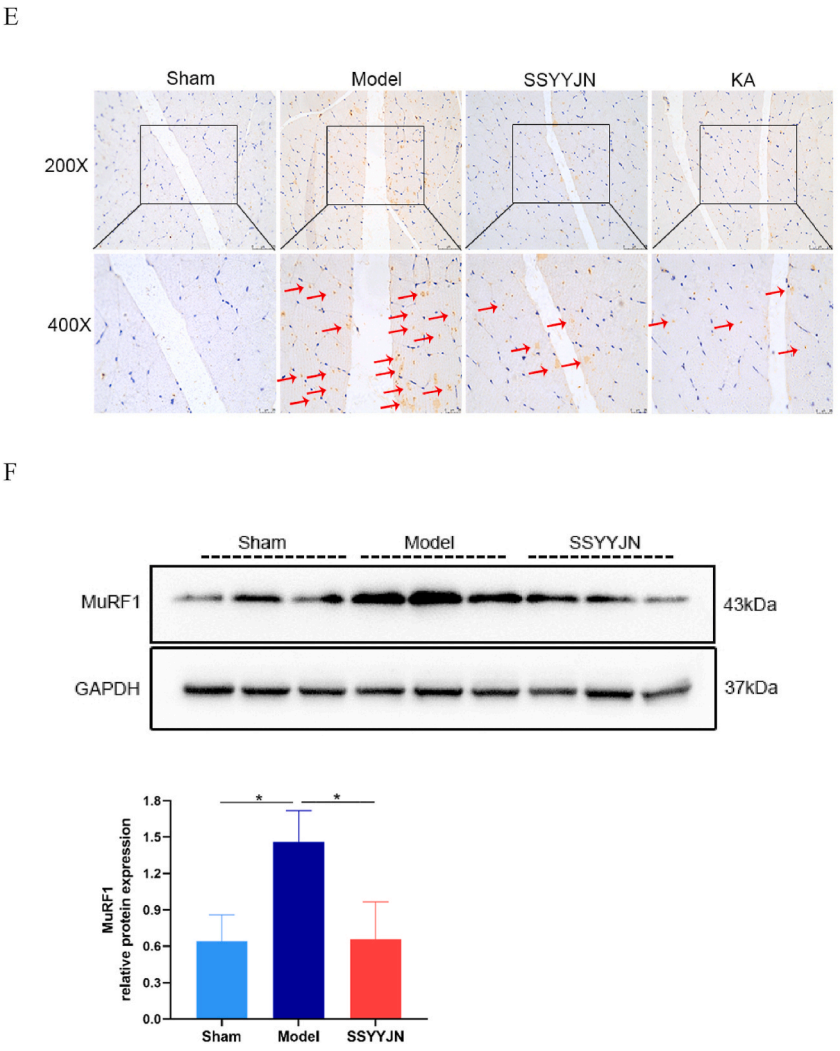

Fig. 3. (*continued*).

Secondly, SSYYJN ameliorated CKD-associated muscle atrophy in rats. This was consistent with previously reported results. As direct indicators of muscular atrophy, we measured body weight, muscle weight and muscle fiber cross-sectional area. The results were consistent with the previous report.[27,28] The body weight of rats in the model group were significantly reduced ($P < 0.01$) at the beginning of treatment when compared with the sham group although there was no significant difference ($P > 0.05$) when compared to the SSYYJN and KA groups. After treatment, the body weights of the SSYYJN and KA groups was significantly increased ($P < 0.05$ or $P < 0.01$) when compared with the model group (Fig. 3A). Furthermore, the ratio of GA and TA muscle weight to body weight showed similar trends ($P < 0.01$; Fig. 3B and C). The cross-sectional area of muscle fibers in the model group was significantly smaller ($P < 0.01$) than that in the sham group. Following SSYYJN and KA treatment, the cross-sectional area of muscle fibers was increased ($P < 0.01$) when compared with the model group (Fig. 3D). MuRF1 is an important indicator of muscle atrophy. We measured the expression of MuRF1 by IHC staining and WB. The levels of MuRF1 were increased ($P < 0.05$) in the TA muscles of rats in the model group; these increases were inhibited ($P < 0.05$) by the administration of SSYYJN (Fig. 3E and F). These results showed that SSYYJN ameliorated skeletal muscle atrophy in rats with CKD-induced muscle atrophy.

At the same time, we found that CKD-induced muscle atrophy occurred in ferroptosis, and SSYYJN inhibited ferroptosis. We next determined the levels of markers of ferroptosis, including iron, NADPH, MDA, GSH, ROS and Gpx4. We found that there was significant iron accumulation ($P < 0.01$) in the TA muscle of the model group (Fig. 4A). Consistent with this result, the model group had a higher level of muscular MDA ($P < 0.01$; Fig. 4B) as well as significantly lower levels of muscular GSH ($P < 0.01$; Fig. 4C) and NADPH ($P < 0.01$; Fig. 4D) when compared to the sham group. All these changes were rescued ($P < 0.05$ or $P < 0.01$) by treatment with SSYYJN. Furthermore, the levels of ROS in each group were detected by fluorescence staining; ROS levels in the model group were significantly higher ($P < 0.01$) than those in the sham group, but decreased ($P < 0.01$) after SSYYJN treatment (Fig. 4E). Next, we measured the level of Gpx4 by WB and RT-qPCR and found that Gpx4 levels were markedly decreased ($P < 0.01$ or $P < 0.05$) in the model group but

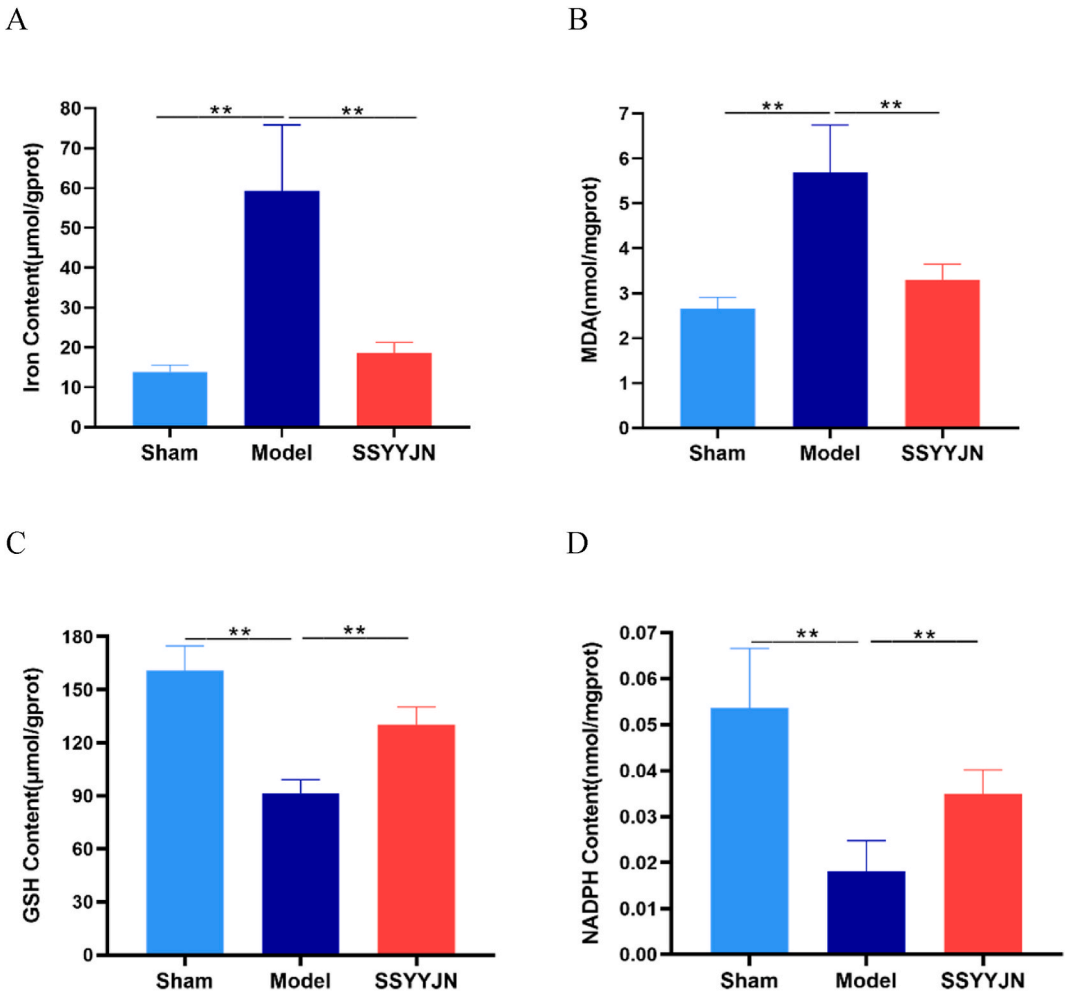

Fig. 4. SSYYJN inhibited the occurrence of ferroptosis in rats with CKD-induced muscle atrophy. (A) Iron levels, (B) MDA levels, (C) GSH levels and (D) NADPH levels in the TA muscles. (E) Representative images of IF staining for ROS (200X) and quantitative analysis. (F) Representative bands for Gpx4 and GAPDH proteins, and statistical analysis of Gpx4 protein expression levels Data are presented as mean. (G) Statistical analysis of Gpx4 mRNA expression. Data are presented as mean ± SD for 3–8 rats in each group. *P < 0.05, **P < 0.01.

was increased (P < 0.05) after SSYYJN administration (Fig. 4F–G).

3.3. Network pharmacology analysis of the molecular mechanisms responsible for the inhibitory action of SSYYJN on ferroptosis

The previous results observed that CKD-induced muscle atrophy occurred ferroptosis, but the mechanism of action is not clear, and this experiment predicts the signaling pathway of SSYYJN acting on ferroptosis by network pharmacology. A total of 130 active components of SSYYJN were identified by screening the TCMSP database: 5 Baizhu, 8 Dahuang, 2 Danggui, 4 Dangshen, 16 Duzhong, 1 Fuling, 81 Gancao, 13 Huangqi and 10 Sharen (Table S3). Furthermore, 961 potential targets of the active compounds were identified by searching the Swiss Target Prediction website; this allowed us to construct a "SSYYJN compound-target" network (Fig. 5A).

After searching for the targets in the corresponding database and removing duplicate values, a total of 14,000 CKD-PEW related targets and 227 ferroptosis-related genes were identified. By taking the intersection of the three sets, a total of 43 common targets were obtained (Fig. 5B). A PPI network was then constructed based on the degree value (Fig. 5C). HIF-1α was identified as the most significant hub gene.

GO enrichment analysis of the 43 common genes found that the biological processes mainly involved response to nutrient level, the regulation of small molecule metabolic processes and ROS metabolic processes. Cell components mainly included glutamatergic synapse and transcription regulator complex. Molecular functional analysis suggested that the common targets are mainly involved in DNA-binding transcription and oxidoreductase activity. KEGG pathway analysis revealed that the hub targets were mainly enriched in the HIF-1α signaling pathway, thus suggesting that HIF-1α signaling pathway regulation may be the major process by which SSYYJN

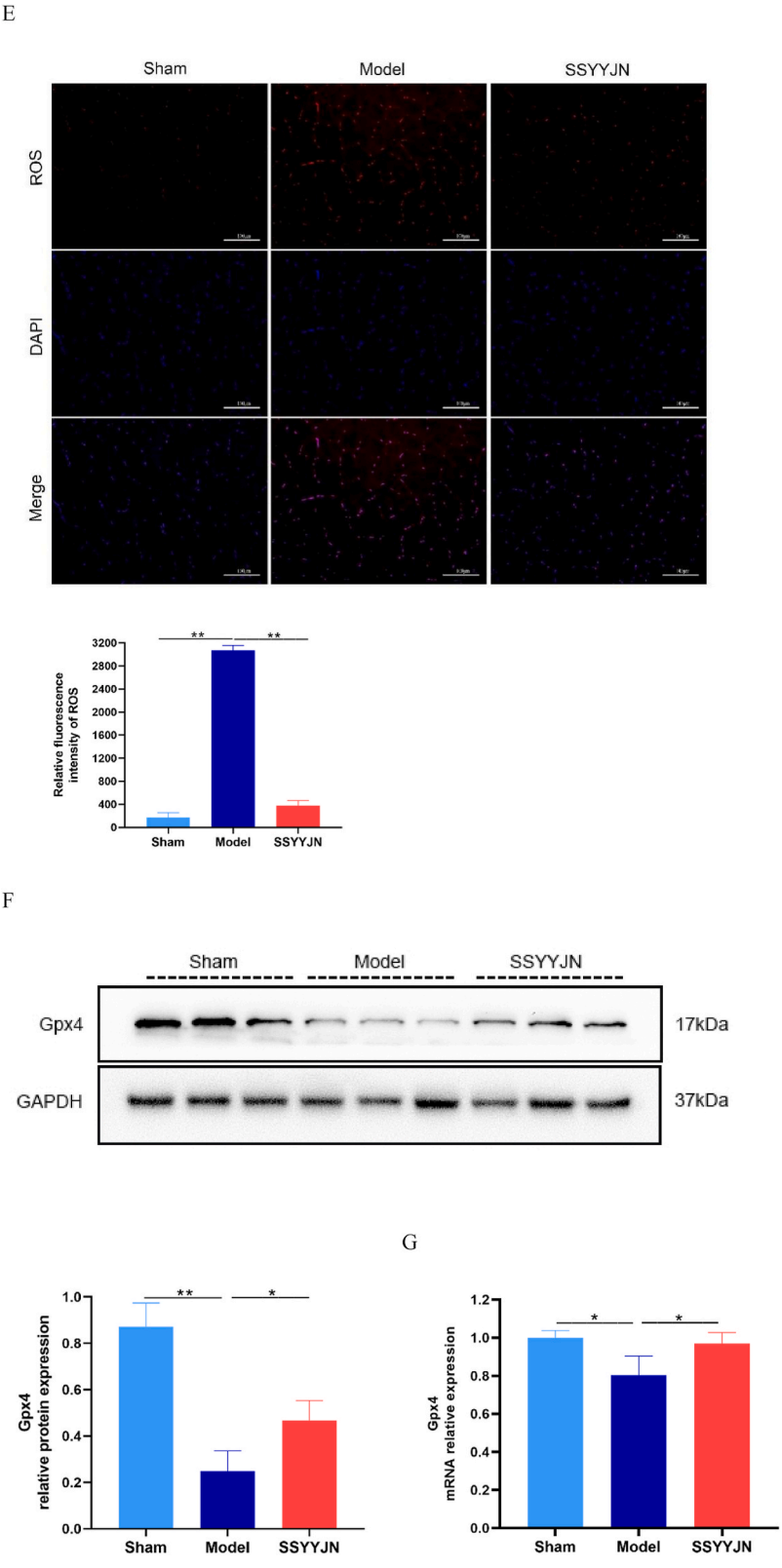

Fig. 4. (*continued*).

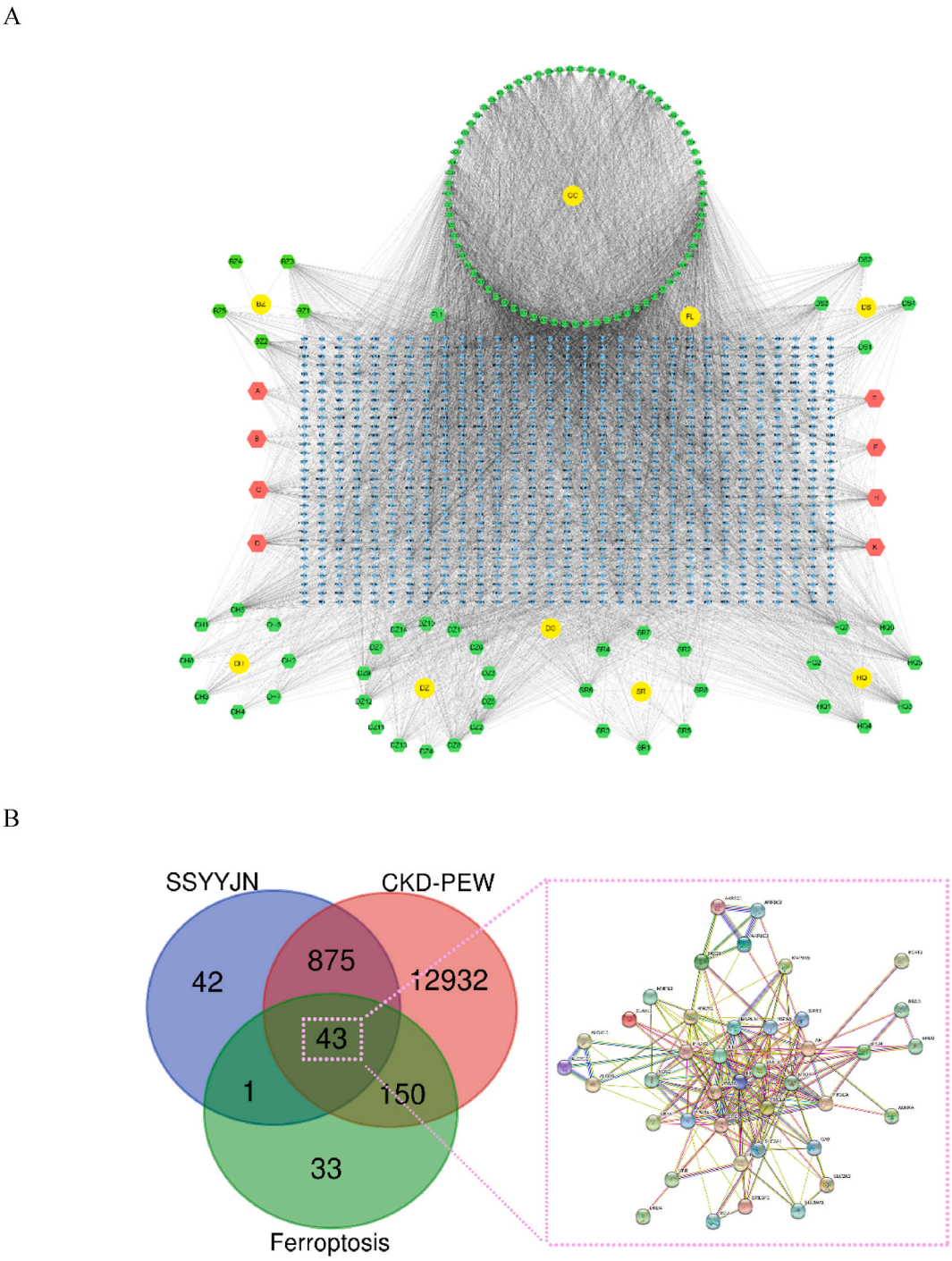

Fig. 5. Network pharmacology analysis was used to identify the molecular mechanisms underlying the inhibitory action of SSYYJN on ferroptosis. (A) An herb-compound-target network for SSYYJN. The yellow circle represents the herbs, the green hexagons represent the active compounds and the blue diamond represent the target. (B) Venn diagram showing the common genes associated with SSYYJN, CKD-PEW and ferroptosis. (C) A PPI network of the common genes; the degree value of the HIF-1α gene was the highest. (D) Bubble diagram for enriched GO terms and KEGG pathways of common genes.. (For interpretation of the references to colour in this figure legend, the reader is referred to the Web version of this article.)

C

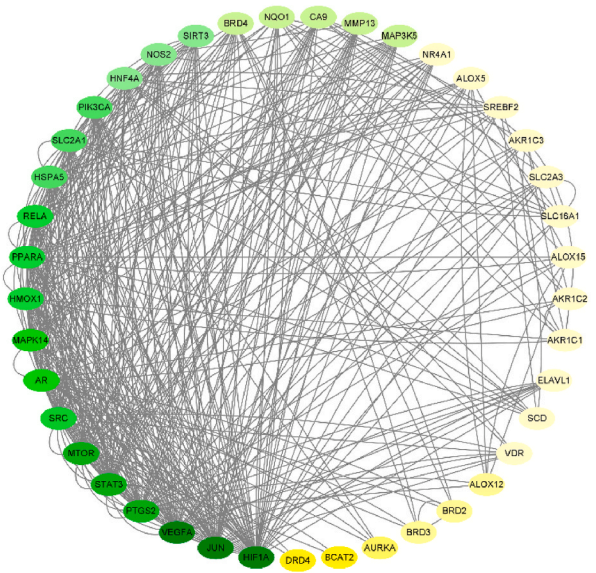

D

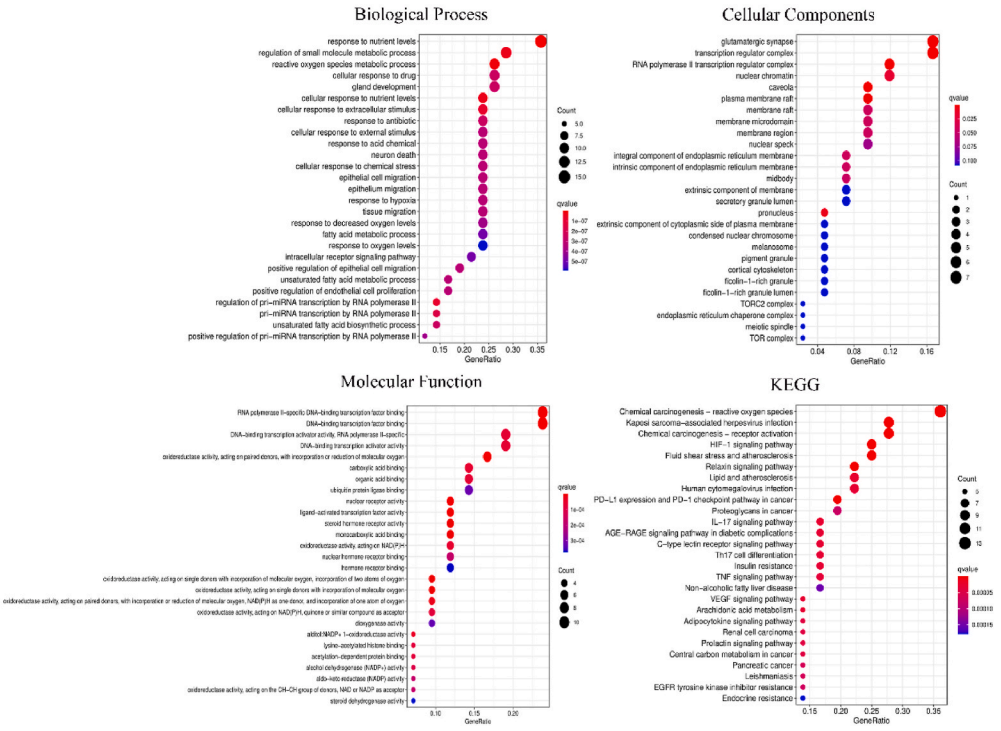

Fig. 5. (*continued*).

inhibited ferroptosis in CKD-induced muscle atrophy (Fig. 5D).

3.4. SSYYJN treatment activated the HIF-1α/SLC7A11 signaling pathway in rats with CKD-induced muscle atrophy

As a transcription factor, HIF-1α can activate the expression of SLC7A11 [20]. The knockout of HIF-1α can significantly reduce the expression levels of SLC7A11 in rats [21,22]. Therefore, we hypothesized that the HIF-1α/SLC7A11 pathway may be involved in the inhibitory action of SSYYJN on ferroptosis. We determined the levels of HIF-1α protein and mRNA and found that the expression levels of HIF-1α were significantly reduced ($P < 0.01$) in the model group but were increased ($P < 0.01$) in the SSYYJN group (Fig. 6A and C).

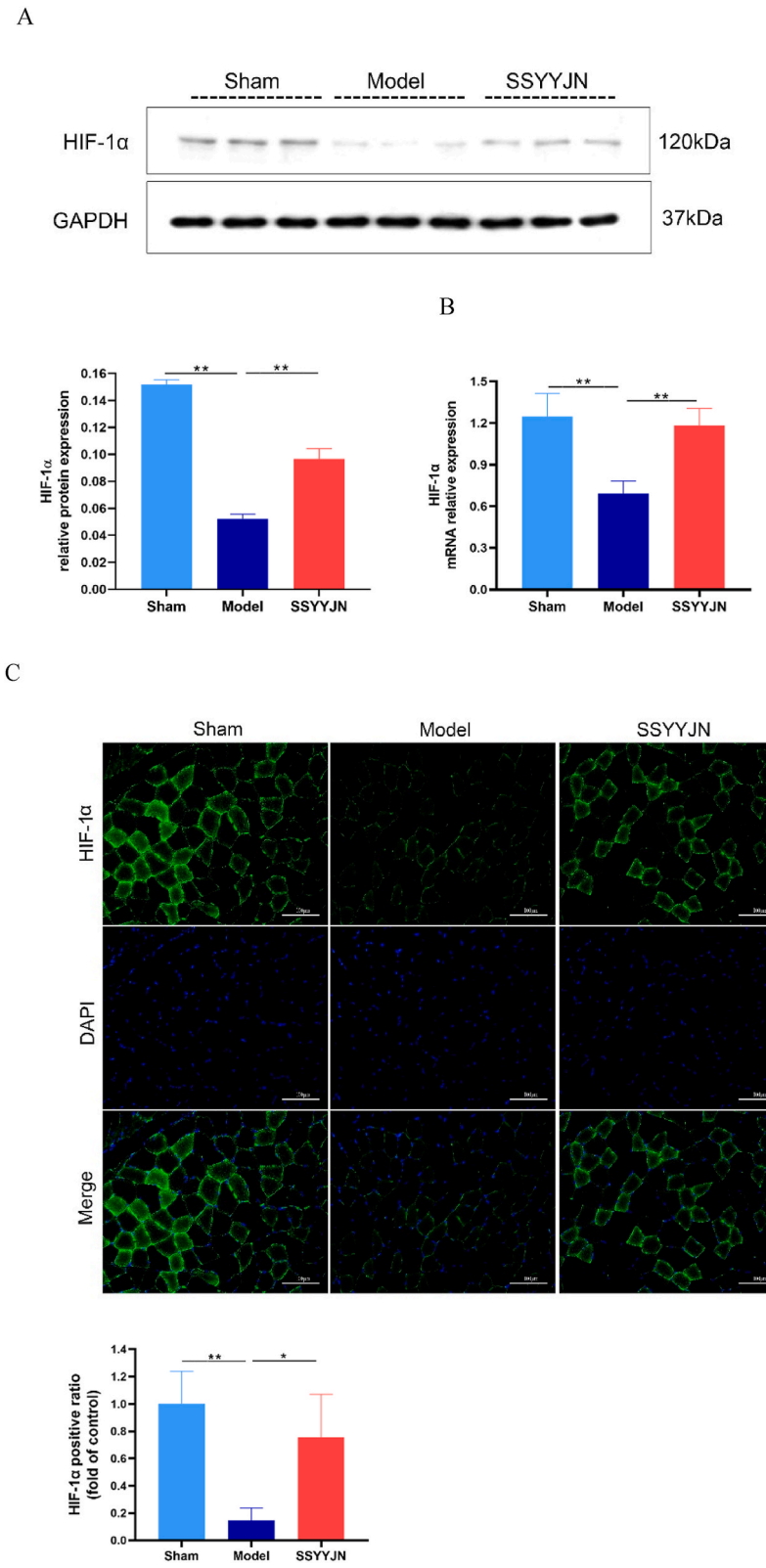

Fig. 6. SSYYJN activated the HIF-1α/SLC7A11 signalling pathway. (A) Representative bands of HIF-1α and GAPDH protein and statistical analysis of WB data. (B) Representative fluorescence images (200X) of HIF-1α (green) and nuclei (blue) along with semi-quantitative analysis. (C) Statistical analysis of HIF-1α mRNA expression. (D) Representative bands for SLC7A11 and GAPDH proteins, and statistical analysis of SLC7A11 protein

expression levels. (E) Statistical analysis of SLC7A11 mRNA expression. Data are presented as mean ± SD for 3 rats in each group. *P < 0.05, **P < 0.01.. (For interpretation of the references to colour in this figure legend, the reader is referred to the Web version of this article.)

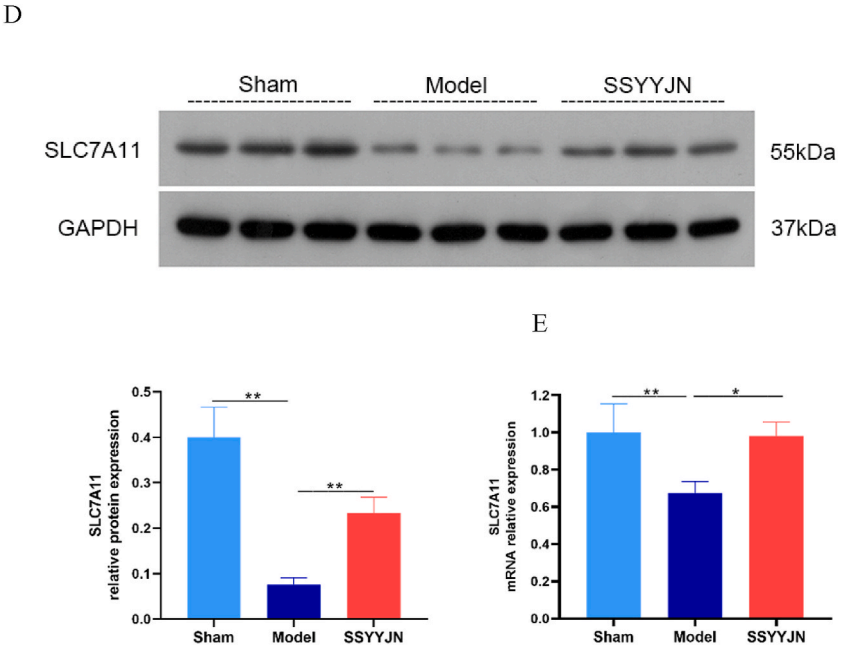

Fig. 6. (*continued*).

HIF-1α immunofluorescence showed the same trend as for WB (P < 0.01 or P < 0.05; Fig. 6B). Next, we measured the level of SLC7A11 by WB and RT-qPCR, which is a known regulator of ferroptosis. We found that SLC7A11 level was markedly decreased (P < 0.01) in the model group but was increased (P < 0.01) after SSYYJN administration (Fig. 6D–E). Overall, these results suggested that SSYYJN can activate the HIF-1α/SLC7A11 signaling pathway.

4. Discussion

We used UPLC-Q-Orbitrap HRMS to systematically analyze the chemical components of SSYYJN for the first time. A total of 42 compounds of SSYYJN were identified, including 14 organic acids and their glycosides, 7 anthraquinone, 7 flavonoids, 2 tannins, 2 alkaloids, 2 triterpenoids, 2 phenylpropan-oid, 1 amino acid, 1 lignans and 4 others. Formononetin, Calycosin, Gallic Acid, Catechin, Ononin, Liquiritin, and Liquiritigenin were some of the compounds identified. Studies have confirmed that Formononetin and Calycosin can improve skeletal muscle atrophy in CKD [23,24]. Gallic Acid has been shown to significantly reduce muscle atrophy [25]. Catechin has been shown to enhance skeletal muscle regeneration and repair [26]. Studies have found that Ononin, Liquiritin and Liquiritigenin can promote the proliferation and differentiation of myoblasts and enhance the diameter of muscle fibers [27]. In summary, SSYYJN contains a number of ingredients that can alleviate skeletal muscle atrophy. It may be an effective prescription to improve CKD associated muscle atrophy.

Muscle atrophy is one of the main complications of CKD. As a recognized model, 5/6 nephrectomy rats are often used in studies of CKD [28]. This model is characterized by increased levels of Scr, BUN and Cystatin C just 8 weeks after surgery [29,30]. In the present study, the CKD model was established by performing 5/6 nephrectomy on SD rats. CKD patients are known to be more susceptible to muscle atrophy, a common feature of all stages of CKD [31]. a low protein diet is also an important factor underlying the occurrence of this complication. To be consistent with the cause of muscle atrophy in CKD patients, we provided our animal models with a 4 % tyrosine diet, a low protein diet, after 5/6 nephrectomy to establish a model of muscle atrophy related to CKD. Seven weeks after surgery, we observed a significant increase in the levels of Scr and a reduction in the levels of ALB and Hb. Interestingly, we did not observe an increase in the levels of BUN in the model group. This may be due to the fact that a low-protein diet can reduce the production of nitrogen (N)-derived products, including BUN, and is clinically used to relieve uremia symptoms in CKD patients [32]. KA is a compound amino acid preparation developed by Fresenius, a German company that is currently the only effective drug for the treatment of CKD-PEW. In this study, we used KA as a positive control.

Ubiquitination is vital for cell metabolism and participates in the process of cell proliferation, differentiation and death [33]. An increasing body of evidence indicates that ubiquitination is associated with ferroptosis [34,35]. As an E3 ubiquitin ligase, MuRF1 is known to be involved in the process of protein ubiquitination. Researchers have also found that MuRF1 is involved in the process of protein decomposition in the skeletal muscle and is a specific marker of muscle atrophy [36]. In the case of skeletal muscle atrophy, the levels of MuRF1 are increased significantly [37]. Consistent with previous observations, our study showed that the levels of MuRF1

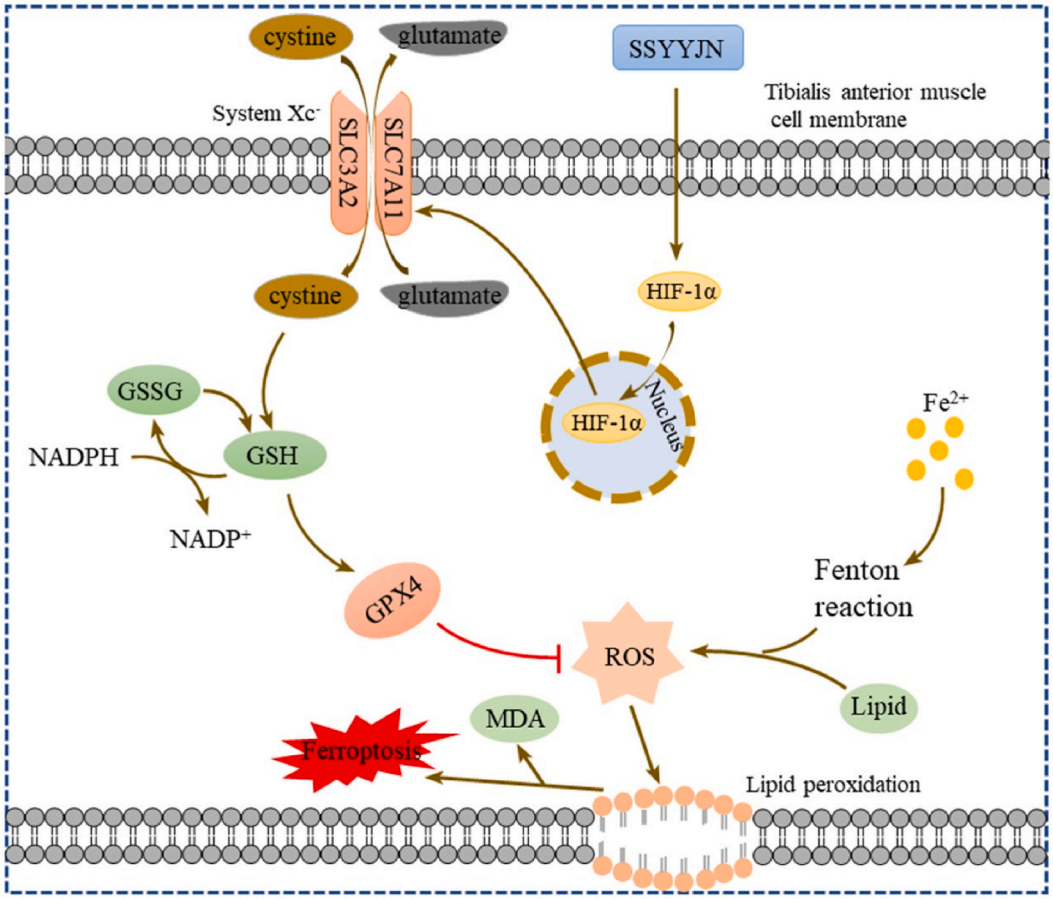

Fig. 7. SSYYJN ameliorates CKD-induced muscle atrophy by inhibiting ferroptosis in tibialis anterior muscle cell via HIF-1α/SLC7A11 pathway. Treatment with SSYYJN induces an increase in HIF-1α, which in turn promotes SLC7A11 expression, then leads to the increase of Gpx4, GSH and the decrease of ROS, and ultimately inhibits muscle cell ferroptosis.

protein were significantly increased in rats with CKD-induced muscle atrophy. Notably, SSYYJN inhibited the expression of MuRF1. These results (Fig. 4A–F) indicate that SSYYJN can effectively relieve skeletal muscle atrophy.

Ferroptosis is the result of excessive ROS production in cells and is caused by an increase in the intracellular concentration of iron [38,39]. Lipid peroxidation is the oxidation of polyunsaturated fatty acids in the membranes of cells or organelles by intracellular ROS [40]. MDA is the main aldehyde product of lipid peroxidation [41]. The protective mechanism exhibited by cells against oxidative stress injury in ferroptosis is multi-faceted. The synthesis of antioxidants, such as GSH and NADPH, is the main method of defense against ferroptosis. Studies have shown that the levels of NADPH in ferroptotic cells are significantly reduced [42]. GSH metabolism capacity is commonly considered as being positively correlated with ferroptosis sensitivity [43]. Previous studies have identified ferroptosis in atrophic skeletal muscle. Our findings also indicated that ferroptosis is activated in CKD-induced muscle atrophy. This event is coupled with labile iron accumulation, reduced levels of GSH and NADPH, and increased levels of ROS and MDA; these have been proven to represent effective markers of ferroptosis in previous studies [44]. We demonstrated that SSYYJN has an anti-ferroptosis effect on CKD-PEW. To further clarify the molecular mechanisms by which SSYYJN can inhibit ferroptosis, we performed network pharmacology analysis. We identified 43 core targets of SSYYJN in the treatment of CKD-PEW by targeting ferroptosis and highlighted HIF-1α as the most significant hub target. Thus, the HIF-1α/SLC7A11 signaling pathway may be the main mechanism by which SSYYJN exerts therapeutic action on CKD-PEW.

SLC7A11 is a major subunit of the cell membrane transporter system Xc− which is known to be involved in the regulation of intracellular redox homeostasis. Cystine is transported into cells through the Xc− system and is then reduced to cysteine to promote GSH synthesis [45]. GSH-dependent Gpx4 can inhibit the occurrence of ferroptosis by catalyzing the reduction reaction of lipid peroxide. As a heterodimer, HIF-1 consists of an α subunit that responds to oxygen and a structurally expressed β subunit. The function of HIF-1 mainly depends on the oxygen-dependent proteolysis of α-subunits [46]. Studies have found that HIF-1α can influence the expression of SLC7A11 to participate in the regulation of ferroptosis [47]. In the current study, we observed that the expression of HIF-1α was down-regulated in rats with CKD-induced muscle atrophy. After the administration of SSYYJN, the expression of HIF-1α was up-regulated in the SSYYJN group. The trend for HIF-1α immunofluorescence was consistent with the WB and RT-qPCR results for

HIF-1α. These results confirmed the predictions arising from our network pharmacology study. WB analysis further confirmed that the levels of Gpx4 and SLC7A11 proteins were lower in the model group than in the sham group but were higher in the SSYYJN group. Furthermore, the results of RT-qPCR for Gpx4 and SLC7A11 were consistent with those arising from WB. These results indicate that SSYYJN can restrain ferroptosis in CKD-induced muscle atrophy by activating the HIF-1α/SLC7A11 pathway (Fig. 7). This illustrates that manipulation of the HIF-1α/SLC7A11 signaling pathway can induce ferroptosis in CKD-induced muscle atrophy and that the inhibition of ferroptosis is one of the mechanisms by which SSYYJN exerts therapeutic effects in CKD-induced muscle atrophy. Although we analyzed the active components of the entire formulation, the monomeric components of SSYYJN that inhibit ferroptosis have not yet been identified.

5. Conclusion

In summary, the present study provides 42 major compounds and qualification of different contents for quality control of SSYYJN. Treatment with SSYYJN decreased Scr, Cystatin C, MuRF1, increased the cross-sectional area of muscle fibers, and improved renal pathological damage in the chronic kidney disease-associated muscle atrophy rats; In terms of antioxidant and ferroptosis, treatment with SSYYJN increased GSH, NADPH, Gpx4, decreased iron, MDA and ROS. Furthermore, SSYYJN treatment increased expression of HIF-1α, SLC7A11. In conclusion, we provide evidences that SSYYJN can ameliorate CKD-induced muscle atrophy by inhibition of skeletal muscle cell of ferroptosis through upregulating the HIF–1α/SLC7A11 pathway.

CRediT authorship contribution statement

Liliang Ju: Writing – original draft, Investigation. **Jianxin Diao:** Writing – review & editing, Funding acquisition. **Jiaxing Zhang:** Formal analysis, Xinyao Xu, Writing – review & editing. **Fahong Dai:** Methodology. **Hong Zhou:** Methodology. **Zhongxiao Han:** Resources. **Rong Hu:** Data curation. **Tingting Pei:** Data curation. **Fujing Wang:** Formal analysis. **Zhuoen He:** Formal analysis. **Xiuqiong Fu:** Resources. **Mingqing Wang:** Funding acquisition. **Wei Xiao:** Project administration, Funding acquisition. **Yun Ma:** Project administration, Investigation, Conceptualization.

Declaration of competing interest

The authors declare that they have no known competing financial interests or personal relationships that could have appeared to influence the work reported in this paper.

Acknowledgements

This work was supported by the National Natural Science Foundation of China under Grant 81973804, 82004336, 82074257 and 82174322; Youth Qihuang scholar program of the State Administration of traditional Chinese Medicine; the Natural Science Foundation of Guangdong Province under Grant 2019A1515011034; Guangdong Administration of Traditional Chinese Medicine under Grant 20200505160744.

Abbreviations

SSYYJN Shenshuai Yingyang Jiaonang
CKD chronic kidney disease
UPLC-Q-Orbitrap HRMS ultrahigh-performance liquid chromatography quadrupole orbitrap high-resolution mass spectrometry
PEW protein energy wasting
GSH glutathione
SLC7A11 solute carrier family 7 member 11
ROS reactive oxygen species
MDA malondialdehyde
NADPH nicotinamide adenine dinucleotide phosphate
Gpx4 glutathione peroxidase 4
TCM traditional Chinese medicine;
HESI heated electrospray ion source
Scr serum creatinine;
BUN blood urea nitrogen
ALB albumin
Hb hemoglobin
KA compound α-keto acid tablet;
BSA bovine serum albumin
TCMSP traditional Chinese medicine systems pharmacology database
OB oral bioavailability
DL, drug-likeness

PPI	protein-protein interaction
GO	gene ontology
KEGG	kyoto encyclopedia of genes and genomes
WB	western blot
MuRF1	muscle ring-finger-1
HIF-1α	hypoxia-inducible factor 1-alpha

Appendix A. Supplementary data

Supplementary data to this article can be found online at https://doi.org/10.1016/j.heliyon.2024.e29093

References

[1] A. Levin, M. Tonelli, J. Bonventre, et al., Global kidney health 2017 and beyond: a roadmap for closing gaps in care, research, and policy, Lancet 390 (10105) (2017) 1888–1917.
[2] K. Matsushita, M. van der Velde, B.C. Astor, et al., Association of estimated glomerular filtration rate and albuminuria with all-cause and cardiovascular mortality in general population cohorts: a collaborative meta-analysis, Lancet 375 (9731) (2010) 2073–2081.
[3] J.J. Carrero, P. Stenvinkel, L. Cuppari, et al., Etiology of the protein-energy wasting syndrome in chronic kidney disease: a consensus statement from the International Society of Renal Nutrition and Metabolism (ISRNM), J. Ren. Nutr. 23 (2) (2013) 77–90.
[4] K. Jiang, M.S. Singh, A. Slee, et al., Differences between anthropometric and bioimpedance measurements of muscle mass in the arm and hand grip and pinch strength in patients with chronic kidney disease, Clin Nutr 40 (1) (2021) 320–323.
[5] S. Bataille, M. Serveaux, E. Carreno, et al., The diagnosis of sarcopenia is mainly driven by muscle mass in hemodialysis patients, Clin Nutr 36 (6) (2017) 1654–1660.
[6] A. Sabatino, L. Cuppari, P. Stenvinkel, et al., Sarcopenia in chronic kidney disease: what have we learned so far? J. Nephrol. 34 (4) (2021) 1347–1372.
[7] V.R. Rajan, W.E. Mitch, Muscle wasting in chronic kidney disease: the role of the ubiquitin proteasome system and its clinical impact, Pediatr. Nephrol. 23 (4) (2008) 527–535.
[8] J. Lv, Y. Li, S. Shi, et al., Skeletal muscle mitochondrial remodeling in heart failure: an update on mechanisms and therapeutic opportunities, Biomed. Pharmacother. 155 (2022) 113833.
[9] Q. Xue, D. Yan, X. Chen, et al., Copper-dependent autophagic degradation of GPX4 drives ferroptosis, Autophagy 19 (7) (2023) 1982–1996.
[10] R. Skouta, S.J. Dixon, J. Wang, et al., Ferrostatins inhibit oxidative lipid damage and cell death in diverse disease models, J. Am. Chem. Soc. 136 (12) (2014) 4551–4556.
[11] H. Ding, S. Chen, X. Pan, et al., Transferrin receptor 1 ablation in satellite cells impedes skeletal muscle regeneration through activation of ferroptosis, J Cachexia Sarcopenia Muscle 12 (3) (2021) 746–768.
[12] M. Yoshida, S. Minagawa, J. Araya, et al., Involvement of cigarette smoke-induced epithelial cell ferroptosis in COPD pathogenesis, Nat. Commun. 10 (1) (2019) 3145.
[13] Y. Xie, W. Hou, X. Song, et al., Ferroptosis: process and function, Cell Death Differ. 23 (3) (2016) 369–379.
[14] S.J. Dixon, K.M. Lemberg, M.R. Lamprecht, et al., Ferroptosis: an iron-dependent form of nonapoptotic cell death, Cell 149 (5) (2012) 1060–1072.
[15] K. Shimada, R. Skouta, A. Kaplan, et al., Global survey of cell death mechanisms reveals metabolic regulation of ferroptosis, Nat. Chem. Biol. 12 (7) (2016) 497–503.
[16] J. Mao, Y. Li, S. Li, et al., Bufei Jianpi granules reduce quadriceps muscular cell apoptosis by improving mitochondrial function in rats with chronic obstructive pulmonary disease, Evid Based Complement Alternat Med 2019 (2019) 1216305.
[17] Y. Kishida, S. Kagawa, J. Arimitsu, et al., Go-sha-jinki-Gan (GJG), a traditional Japanese herbal medicine, protects against sarcopenia in senescence-accelerated mice, Phytomedicine 22 (1) (2015) 16–22.
[18] R. Hu, M.Q. Wang, Y.Y. Liu, et al., Anti-inflammatory effect of renal failure nutrition capsule on vascular injury in microinflammatory state in 5/6 nephrectomy rats with chronic renal failure, Guangdong Medical Journal 37 (22) (2016) 3345–3348.
[19] D.T. Wang, L. Lu, Y. Shi, et al., Supplementation of ketoacids contributes to the up-regulation of the Wnt7a/Akt/p70S6K pathway and the down-regulation of apoptotic and ubiquitin-proteasome systems in the muscle of 5/6 nephrectomised rats, Br. J. Nutr. 111 (9) (2014) 1536–1548.
[20] M. Yang, P. Chen, J. Liu, et al., Clockophagy is a novel selective autophagy process favoring ferroptosis, Sci. Adv. 5 (7) (2019) w2238.
[21] S. Ananth, E. Babu, R. Veeranan-Karmegam, et al., Induction of the cystine/glutamate exchanger SLC7A11 in retinal pigment epithelial cells by the antipsoriatic drug monomethylfumarate, Invest. Ophthalmol. Vis. Sci. 54 (3) (2013) 1592–1602.
[22] C.H. Hsieh, Y.J. Lin, W.L. Chen, et al., HIF-1alpha triggers long-lasting glutamate excitotoxicity via system x(c)(-) in cerebral ischaemia-reperfusion, J. Pathol. 241 (3) (2017) 337–349.
[23] R. Hu, M.Q. Wang, L.Y. Liu, et al., Calycosin inhibited autophagy and oxidative stress in chronic kidney disease skeletal muscle atrophy by regulating AMPK/SKP2/CARM1 signalling pathway, J. Cell Mol. Med. 24 (19) (2020) 11084–11099.
[24] L. Liu, R. Hu, H. You, et al., Formononetin ameliorates muscle atrophy by regulating myostatin-mediated PI3K/Akt/FoxO3a pathway and satellite cell function in chronic kidney disease, J. Cell Mol. Med. 25 (3) (2021) 1493–1506.
[25] F. Felice, M.M. Cesare, L. Fredianelli, et al., Effect of tomato peel extract grown under drought stress condition in a sarcopenia model, Molecules 27 (8) (2022).
[26] P. Li, A. Liu, C. Liu, et al., Role and mechanism of catechin in skeletal muscle cell differentiation, J. Nutr. Biochem. 74 (2019) 108225.
[27] E.J. Lee, S. Shaikh, K. Ahmad, et al., Isolation and characterization of compounds from Glycyrrhiza uralensis as therapeutic agents for the muscle disorders, Int. J. Mol. Sci. 22 (2) (2021).
[28] L. Sun, Q. Yuan, T. Xu, et al., Pioglitazone improves mitochondrial function in the remnant kidney and protects against renal fibrosis in 5/6 nephrectomized rats, Front. Pharmacol. 8 (2017) 545.
[29] W. Jing, A. Nunes, T. Farzaneh, et al., Phosphate binder, ferric citrate, attenuates anemia, renal dysfunction, oxidative stress, inflammation, and fibrosis in 5/6 nephrectomized CKD rats, J Pharmacol Exp Ther 367 (1) (2018) 129–137.
[30] W. Fu, Y. Wang, Z. Jin, et al., Losartan alleviates renal fibrosis by down-regulating HIF-1alpha and up-regulating MMP-9/TIMP-1 in rats with 5/6 nephrectomy, Ren. Fail. 34 (10) (2012) 1297–1304.
[31] M.D. Yu, H.Z. Zhang, Y. Zhang, et al., Relationship between chronic kidney disease and sarcopenia, Sci. Rep. 11 (1) (2021) 20523.
[32] D. Verzola, D. Picciotto, M. Saio, et al., Low protein diets and plant-based low protein diets: do they meet protein requirements of patients with chronic kidney disease? Nutrients 13 (1) (2020).
[33] G. Lu, L. Wang, J. Zhou, et al., A destiny for degradation: interplay between cullin-RING E3 ligases and autophagy, Trends Cell Biol. 31 (6) (2021) 432–444.
[34] J.A. Harrigan, X. Jacq, N.M. Martin, et al., Deubiquitylating enzymes and drug discovery: emerging opportunities, Nat. Rev. Drug Discov. 17 (1) (2018) 57–78.
[35] M. Rape, Ubiquitylation at the crossroads of development and disease, Nat. Rev. Mol. Cell Biol. 19 (1) (2018) 59–70.

[36] D. Wang, J. Chen, X. Liu, et al., Retraction Note: a Chinese herbal formula, Jian-Pi-Yi-Shen decoction, improves muscle atrophy via regulating mitochondrial quality control process in 5/6 nephrectomised rats, Sci. Rep. 11 (1) (2021) 12831.
[37] S.C. Bodine, L.M. Baehr, Skeletal muscle atrophy and the E3 ubiquitin ligases MuRF1 and MAFbx/atrogin-1, Am. J. Physiol. Endocrinol. Metab. 307 (6) (2014) E469–E484.
[38] P. Lei, T. Bai, Y. Sun, Mechanisms of ferroptosis and relations with regulated cell death: a review, Front. Physiol. 10 (2019) 139.
[39] D. Zhao, K. Yang, H. Guo, et al., Mechanisms of ferroptosis in Alzheimer's disease and therapeutic effects of natural plant products: a review, Biomed. Pharmacother. 164 (2023) 114312.
[40] L.J. Su, J.H. Zhang, H. Gomez, et al., Reactive oxygen species-induced lipid peroxidation in apoptosis, autophagy, and ferroptosis, Oxid. Med. Cell. Longev. 2019 (2019) 5080843.
[41] A. Ayala, M.F. Munoz, S. Arguelles, Lipid peroxidation: production, metabolism, and signaling mechanisms of malondialdehyde and 4-hydroxy-2-nonenal, Oxid. Med. Cell. Longev. 2014 (2014) 360438.
[42] K. Shimada, M. Hayano, N.C. Pagano, et al., Cell-line selectivity improves the predictive power of pharmacogenomic analyses and helps identify NADPH as biomarker for ferroptosis sensitivity, Cell Chem. Biol. 23 (2) (2016) 225–235.
[43] J. Zhu, Y. Xiong, Y. Zhang, et al., The molecular mechanisms of regulating oxidative stress-induced ferroptosis and therapeutic strategy in tumors, Oxid. Med. Cell. Longev. 2020 (2020) 8810785.
[44] H. Wang, P. An, E. Xie, et al., Characterization of ferroptosis in murine models of hemochromatosis, Hepatology 66 (2) (2017) 449–465.
[45] B.R. Stockwell, A.J. Friedmann, H. Bayir, et al., Ferroptosis: a regulated cell death nexus linking metabolism, redox biology, and disease, Cell 171 (2) (2017) 273–285.
[46] L.E. Otterbein, M.P. Soares, K. Yamashita, et al., Heme oxygenase-1: unleashing the protective properties of heme, Trends Immunol. 24 (8) (2003) 449–455.
[47] S. Yuan, C. Wei, G. Liu, et al., Sorafenib attenuates liver fibrosis by triggering hepatic stellate cell ferroptosis via HIF-1alpha/SLC7A11 pathway, Cell Prolif. 55 (1) (2022) e13158.

References

[48] Y. Niu, S.F. Wan g, Analysis on chemical constituents in Danggui-Shaoyao-San by LC-Q-TOF-MS and LC-IT-MSn, Chin. Tradit. Herb. Drugs 45 (8) (2014) 1056–1062.
[49] M.Y. Shen, B. Wu, H.Q. Duan, et al., Comparative study on secondary metabolites of Eucommia ulmoides leaves between arboreal forest and leaf forest based on Uplc-Q-Orbitrap HRMS, Natural product research and development (2022) 1–30.
[50] J. Hu, Study on Chemical Components of Danggui Buxue Decoction Based on UPLC-Q-TOF-MS Combined with Diagnostic Ions and Molecular Network strategies [J], Shanxi University, 2021.
[51] S.N. Luo, Z.C. Peng, Q. Fan, et al., Analysis on chemical constituents in Xiao Chengqitang by UPLC-Q-orbitrap-MS, Chin. J. Exp. Tradit. Med. Formulae 27 (23) (2021) 1–10.
[52] T.Y. An, X.H. Chen, M. Zhang, et al., Rapid analysis on chemical constituents from Codonopsis tangshen Oliv. by UPLC coupled with Q-Exactive quadrupole-Orbitrap MS, Chin. Tradit. Herb. Drugs 49 (7) (2018) 1533–1542.
[53] H. Min, T.T. Luo, X.H. Yin, et al., Rapid analysis components of Lingguizhugan decoction with HPLC-Q/TOF-MS, Modern Chinese Medicine 23 (3) (2021) 529–535.
[54] Y. Yan, H. Zhao, L.S. Zou, et al., Chemical constituents of eucommiae cortex by LC-triple TOF MS/MS, J. Chin. Mass Spectrom. Soc. 38 (1) (2017) 146–156.
[55] Q. Zhao, Y.P. Chen, X.S. Cui, et al., Study on multi-compound determination and fingerprint of Rheum palmatum by ultra performance liquid chromatography, Chinese Journal of Pharmaceutical Analysis 38 (10) (2018) 1697–1710.
[56] Q. Huang, Q. Liu, F.Y. Zhang, et al., Active ingredient analysis of Eucommia ulmoides Oliv. in treating diabetic nephropathy by using UPLC-Q-TOF-MS and network pharmacology, Chin. J. New Drugs Clin. Remedies 40 (2021) 460–469, 06.
[57] A. Kang, J.R. Guo, T. Xie, et al., Analysis of the triterpenes in Poria cocos by UHPLC-LTQ-orbitrap MS/MS, Journal of Nanjing University of Traditional Chinese Medicine 30 (6) (2014) 561–565.
[58] C. Fu, C. Chen, G.X. Zhou, et al., Chemical constituents from fruits of Amomum villosum, Chin. Tradit. Herb. Drugs 42 (12) (2011) 2410–2412.
[59] H.S. Shi, X.F. Bi, X.H. Shi, Analysis on the chemical constituents of flavones and saponin in the root and stem leaf of Astragalus membranaceus with ultra-high performance liquid chromatography coupled with hybrid quadrupole-orbitrap mass spectrometry, World Journal of Integrated Traditional and Western Medicine 13 (3) (2018) 357–361.
[60] L.L. Yan, Effective Substances Research of Chemical Composition of Banxia Xiexin Decoction with UPLC/Q-TOF-MSE[J], Peking Union Medical College, 2013.
[61] Y.M. Zhao, S.X. Liu, C.X. Zhang, et al., Analysis on chemical constituents from Glycyrrhizae Radix et Rhizoma by HPLC-Q-TOF-MS, Chin. Tradit. Herb. Drugs 47 (12) (2016) 2061–2068.
[62] J. Zhang, X.J. Xu, W. Xu, et al., Rapid identification of chemical constituents from Codonopsis radix by HPLC-LTQ-Orbitrap-MSn, Chin. J. Exp. Tradit. Med. Formulae 21 (9) (2015) 59–63.
[63] L.L. Gao, Studies on the Chemical Constituents and Biological Activity of Rheum Tanguticum Maxim. Ex Balf., Rheum Officinale Baill. And Rheum Palmatum L [J], Peking Union Medical College, 2012.
[64] W.X. Li, W.J. Ni, X.Y. Wang, et al., Prediction and analysis of chemical components, pharmacological action and quality marker (Q-Marker) of Angelica sinensis, Chinese Archives of Traditional Chinese Medicine (2022) 1–19.